PORPHYRIN AND BODIPY MOLECULAR ROTORS AS MICROVISCOMETERS

By

JOSEPH DANIEL KIMBALL III

Bachelor of Science, 2010

Michigan State University

East Lansing, MI, USA

Submitted to the Graduate Faculty of the

College of Science and Engineering

Texas Christian University

in partial fulfillment of the requirements

for the degree of

Doctor of Philosophy

December 2015

PORPHYRIN AND BODIPY

MOLECULAR ROTORS

AS MICROVISCOSMETERS

By

Joseph Daniel Kimball III

Dissertation Approved:

Major Professor

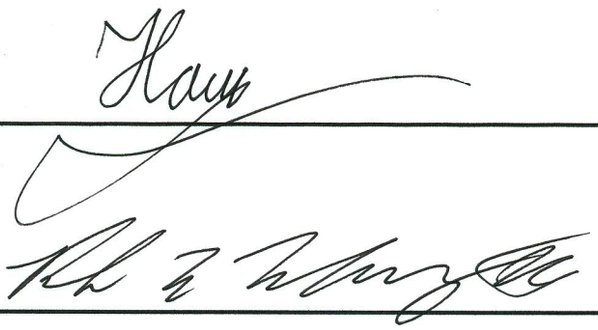

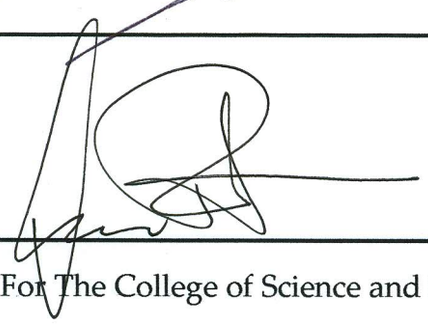

For The College of Science and Engineering

Acknowledgments

I would like to greatly thank my advisor, Dr. Zygmunt (Karol) Gryczynski, for everything he has done for me the last five years. He has taught me to learn, grow, and question everything in the world of physics (and out) as part of a group and independently. I sincerely appreciate his help and guidance over the years. I would also like to thank Dr. Waldek Zerda for his support over the first two years here, along with introducing me to the world of research and teaching.

I would like to express great gratitude to Dr. Sangram Raut. Over the years, he has been the best lab partner / mentor I could imagine. I also want to thank Hung The Doan for his help and support as my good labmate and friend since I've been at TCU. I am also grateful for all the help and discussions with all the graduate students in the physics department and all my collaborators at TCU and around the world.

I am lucky to have had Dr. Sergei Dzyuba, along with Dr. Milan Balaz, for the synthesis and understanding of the dyes I studied in my time here. I am also grateful for the guidance and rapport with everyone from the UNT HSC, including Dr. Ignacy Gryczynski, Dr. Rafal Fudala, Dr. Badri Maliwal, and Dr. Ryan Rich.

I would also like to thank my family and friends for their support over a long journey, especially to my parent's Joe and Colleen Kimball. Without their help, I certainly wouldn't be who and where I am now.

Table of Contents

List of Figures

List of Tables

List of Schemes

List of Abbreviations

Chapter 1

FRET: Förster Resonance Energy Transfer

TICT: Twisted Intramolecular Charge Transfer

ILs: Ionic Liquids

PD: Porphyrin Dimer

BODIPY: boron-dipyroomethene

THF: Tetrahydrofuran

BD: Bodipy dimer / dyad / homodimer

Chapter 2

IC: Internal Conversion

ITC: Intersystem Crossing

QY: Quantum yield

ns: nanoseconds

Φ_f: Quantum Yield

D: Donor

A: Acceptor

Chapter 3

TSCPC: Time Correlated Single Photon Counting

MALDI-TOF: Matrix Assisted Laser Desorption/Ionization-Time of Flight

HPLC: High Performance Liquid Chromatography

DMSO: Dimethylsulfoxide

rpm: revolutions per minute

NA: numerical aperture

EDTA: Ethylenediaminetetraacetic acid

PBS: Phosphate-Buffered Saline

Chapter 4

mPa s: milliPascal seconds

$\langle\tau\rangle_{Int}$: Intensity averaged lifetime

$\langle\tau\rangle_{Amp}$: Amplitude averaged lifetime

° C: Degrees Celsius

cP: centiPoise

DPPC: 1,2-dipalmitoyl-*sn*-glycero-3-phosphocholine

POPC: 1-palmitoyl-2-oleoyl-*sn*-glycero-3-phosphocholine

DMPC: 1,2-dimyristoyl-*sn*-glycero-3-phosphocholine

SKOV3: *Homo sapiens* ovary adenocarcinoma cell line

FLIM: Fluorescence Lifetime Imaging Microscopy

Calu 3: *Homo sapiens* lung adenocarcinoma cell line

DU 125: *Homo sapiens* prostate carcinoma cell line

Chapter 5

EtOH: ethanol

v/v: volume to volume

min.: minutes

FWHM: Full Width Half Maximum

BSA: Bovine Serum Albumin

HSA: Human Serum Albumin

Symbols

ν: frequency

τ: fluorescent lifetime

η: viscosity

Chapter 1: Introduction

1.1 Introduction

Viscosity, a fluid's internal resistance to flow and resist molecular diffusion, is a fundamental property of fluid media. Determining the bulk viscosity of a fluid has been easy to relatively simple to accomplish for many years, yet in the recent decade there has been a focus on techniques to measure a fluid's microviscosity. Microviscosity differs from bulk viscosity such that microviscosity is the friction experienced by a single particle interacting with its micron-sized local environment. Macroscopic methods to evaluate the viscosity are well established, but methods to determine viscosity on the microscale level remains unclear.

Understanding microviscosity is important because it one of the main properties of any fluid and thus has an effect on any diffusion related processes. A variety of mass and signal transport phenomena as well as intermolecular interactions are often governed by viscosity. [1,2,3] As such, it is important to be able to measure/estimate viscosity and detect the changes in viscosity upon exposure to a stimulus. In view of synthetic accessibility, molecular viscometers are attractive probes for sensing the viscosity of various environments.[4-6] Therefore, evaluating the viscosity in various microenvironments using molecular probes is an attractive area of modern research with numerous applications in chemistry, biology and drug discovery.

Measuring microviscosity is typically accomplished using some form of a flow tracer. Deciding beforehand which type to use and their reliability is clearly the most important aspect of the measurement. Various methods have been used, but we want to determine a simple, reliable method to measure microviscosity. Radiological tracers can be used, but efforts using light are safer and offers increased sensitivity. Diffusing-wave spectroscopy from dynamic light scattering can be used, but that is typically used in systems which are completely transparent at high concentrations and depends on the size, shape and morphology of the tracer particles along with the refractive index of the medium. An easier method and more reliable method also using light-fluorescence anisotropy or depolarization, was originally used extensively to determine the rotational correlation time of fluorescent molecules. However, fluorescence anisotropy has a small dynamic range (-0.2 to 0.4) and depends greatly on the polarization effects of the optical set-up being utilized, thus making polarization-based measurements subject to scrutiny to alignment and correction factors. However, anisotropy is not the only fluorescence based technique which can utilized to measure microviscosity.

Molecular rotors offer a simple and reliable method to measure microviscosity. They are fluorescent probes with different fluorescence moieties which can used as a micoviscometer. They are reliable because their fluorescence intensities and lifetimes are linearly related to its surrounding microviscosity and it does not involve any further polarization measurements. They have been used in numerous applications in

ratiometric sensing of analytes, cascade-type energy transfer events and chemical these transformations.[7-10] Arguably, due to the high sensitivity of fluorescence, as well as the potential for high-throughput screening and imaging, the use of fluorescent probes as microviscometers, *provide ample opportunities and advances as to our goal: develop a simple, reliable microviscometer.*

Ionic liquids (ILs) are materials which can be designed to have specific microviscosity. Thus, using ILs which were created to cover a broad range of microviscosities measurement of our fluorophores in these media should give reliable results across a wide range of viscosities not available by traditional molecular organic media (ethanol, glycerol, etc). Ionic Liquids are comprised exclusively of ions, and have phase-transition temperatures at or below room temperature.[11]

Studies on viscosity of ILs using fluorescent dyes has been a subject of interest,[25-27] and the use of fluorescent probes for understanding the structure of ILs, in general, has been recently reviewed.[28] ILs have found numerous and ever-expanding applications in various areas of science and engineering.[11-17] Virtually unlimited structural variations of ILs, which can be obtained via well-developed synthetic routes, are likely to give rise to distinct physicochemical properties such as phase transitions, density, viscosity, polarity, hydrogen bonding abilities, etc.[18] Arguably, these physical properties could have an impact on solutes, and therefore, the ILs can be designed to control the outcome of a given process by simply varying the

structure of cationic and anionic components. This has led to the idea of ILs as designer solvents. The designer solvent ability has been defined as the manipulation of a structure and thus physical property of the IL which can predictably alter the outcome of a given process.[19, 20] As such, this paradigm has been illustrated through several synthetic transformations.[19-21] However, applications demonstrating the designer solvent ability of ILs outside of their use as milieu for synthetic organic transformations appear to be limited. Notably, it was demonstrated that structural changes within either the cation or anion could be used to modulate the conformational flexibility of a small molecule.[22, 23] Possibilities for using neat ILs to control intermolecular interactions have been suggested primarily for cyanine dye self-assemblies.[24]

Fluorescence is one of the most sensitive detection methods available. The phenomenon was first observed hundreds of years ago, developed as a scientific endeavor in the past 100 years, but in the past three decades it has come to be used extremely widely in the biomedical and diagnostics fields. In simple terms, fluorescence occurs when a molecule absorbs a photon, this energy then promotes the molecule an excited state, which then is released as another photon in order to return the molecule to its ground state. This is typically best explained by a Jablonski-Perrin diagram (Fig. 1.1).

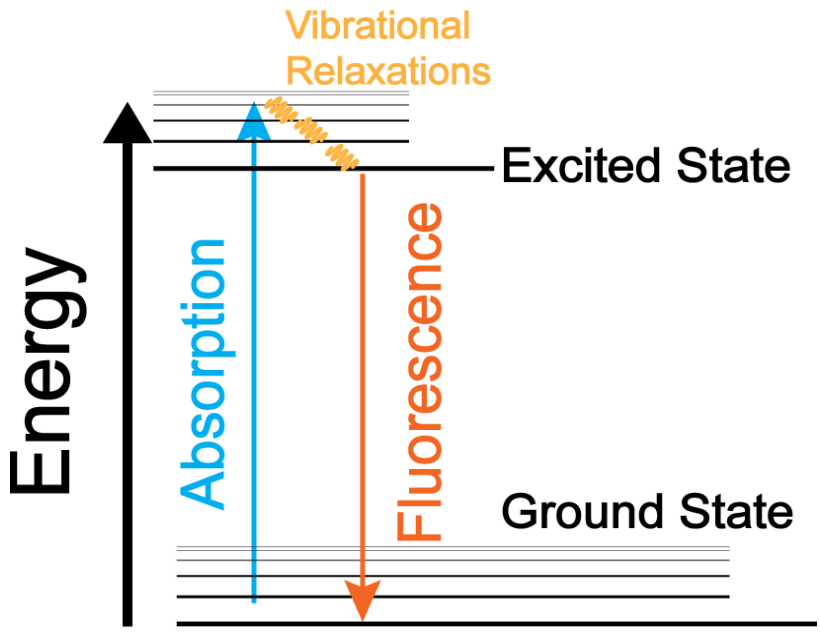

Figure 1.1) Jablonski-Perrin Diagram illustrates the fluorescence process

If a photon of sufficient energy is incident on a molecule, the molecule has a probability to absorb that photon and promote its electronic energy level from the ground state to an excited state, the blue line in Fig. 1.1. Once in its excited state, the energy can be released back in the form of a photon, typically of less energy, through fluorescence (the orange line in Fig. 1.1). The energy can be dissipated non-radiatively (yellow lines in Fig. 1.1) in a variety of ways, most commonly through collisions with other molecules and molecular vibrations. The time it spends in its excited state is known as its fluorescence lifetime.

The spectroscopic properties of the fluorophores, including extinction coefficients, apparent brightness and Stokes shifts, could be tuned via structural and functional modification of the fluorophores. Since many biochemical applications are hindered by

the lack of suitable structurally diverse fluorophores, the access to fluorophores, which rely on facile and modular synthetic approaches allowing for the formation of both homodimeric and heterodimeric systems, might provide a viable solution. Three different molecular rotors were used in this work. *The goal of increasing both the synthesis simplicity and measurement sensitivity of the molecular rotor was one of the main motivations throughout their subsequent development.*

1.4 Porphyrin Dimer

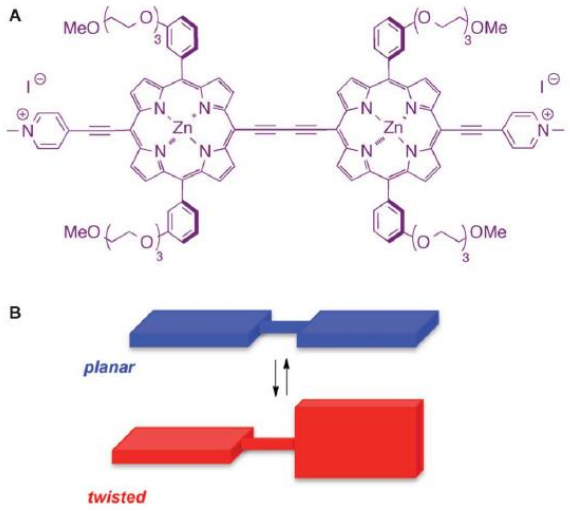

Figure 1.2) Chemical structure (A) and two conformational extremes (B) of **PD**

It was shown that the viscosity of molecular organic media could control the conformation transition of a conjugated porphyrin dimer (**PD**), resulting in an array of conformations with two distinct extremes: a planar and a twisted conformation (Fig. 1.1).[29, 30] This characteristic is unique for this particular probe, as many

fluorescent molecular rotors used for viscosity studies report on viscosity primarily through an emission enhancement[31] or lifetime change,[4] rather than a distinct change in emission wavelength. A linear dependence was observed between the conformational transition preferences of **PD** and viscosity of the media.[30]

The **PD** is a molecular rotor of the type which undergoes TICT and releases this energy radiatively. Importantly, planar and twisted conformations exhibited distinct emission maxima: 720 nm for twisted and 780 nm for planar, which allowed for a facile and straightforward evaluation of the conformational preference of **PD**. Specifically, in non-viscous media, e.g., methanol, the planar conformer was shown to predominate, while in more viscous methanol–glycerol mixtures, the twisted conformation was observed.[30] Thus, **PD** was proposed to be a suitable probe for an investigation of the media's viscosity.

Conversely, viscosity of the media might be viewed as a physical property that could control the conformation transition of **PD**. Because the viscosity of ILs can easily be tuned by varying the structure of the cationic and anionic counterparts,18 we investigated whether the conformational preference of **PD** would be altered as a consequence of changes in the viscosity due to variances in the IL structure. As such, this could also be used as a corroboration of the designer solvent ability of ILs,[19, 20] as well as a demonstration of the distinct nature of ILs as compared to the molecular solvents.

However, the synthesis of **PD** utilizes a time and material consuming 14 step process, leaving us to desire to obtain a molecular rotor which we can create and use for a large variety of measurements. BODIPY dyads and triads molecular rotors were designed and used because they can be synthesized in two and three steps, respectively.

1.5 BODIPY Rotors

BODIPY (boron-dipyrromethene) dyes are versatile fluorophores that have received a significant amount of attention after its first synthesis in 1968[32] due to their wide-spread applications in chemical, biological, and materials sciences, for example as pH sensor, peptide conjugates and as a laser dye. Importantly, the photophysical properties of these dyes can be tuned via structural modifications of the boron-dipyrromethene scaffold.[33-35] As such, BODIPY dyes offer a number of advantages over other types of fluorescent dyes, owing to the relatively facile synthetic manipulations that allow for the incorporation of various moieties in a fairly straightforward and modular manner, although it is not always very efficient and/or economical.

Several BODIPY-based viscometers have been recently reported, as shown in Fig. 1.3 A,B, and D.[36] Typically, the rotor-moiety is attached at the meso-position of the BODIPY scaffold which allows for a rotation around the single C-C bond in the

meso position. In general, an increase in viscosity should suppress the rotation of the substituents around the BODIPY core in the exited state, and as a result suppress the non-radiative decay, which will lead to an increase in emission intensity, quantum yield, and lifetime.[4, 37-42] It could be assumed that the photophysical properties of BODIPY dyes, lifetimes in particular, are insensitive to variations in the polarity and pH of the media, thus making these dyes viable for monitoring viscosity changes within different types of media. Specifically, the lifetimes of BODIPY viscometers (typically in the ns range) showed a linear correlation with the viscosity in the 15–1000 mPa s range. The main application of these rotors has been the evaluation of viscosity of molecular solvents as well as cellular environments.[4, 38, 42-46] Several examples for using BODIPY-based rotors as fluorescent pressure sensors have also been reported.[43,47]

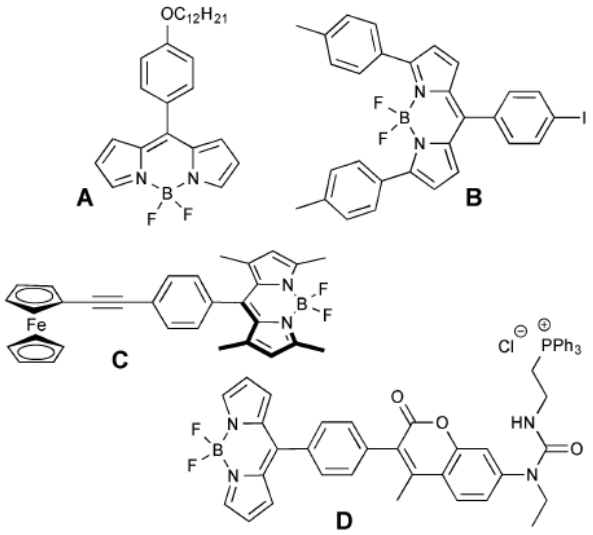

Figure 1.3) Some representative examples of BODIPY based viscometers; A) ref 38; B) ref 48 C) ref 49 D) ref 50

Additionally, temperature-dependent changes in the microviscosity of poly(N-isopropylacrylamide-4-chloromethylstyrene) polymers were recorded by covalently attaching a BODIPY fluorophore to the polymer's side chain.[51] Also, an effect of the so-called remote substituents, i.e., aromatic (phenyl and tolyl) moieties in the 3- and 5-positions of the BODIPY motif (Fig. 1.2 B) on the ability to respond to changes in the media's viscosity was evaluated in a series of homologous, straight chain alcohols with increasing viscosity (ca. 0.5–10 mPa s).[48]

Only a few examples of BODIPY dyads as molecular viscometers have been reported. Specifically, the fluorescence intensity as well as quantum yield of a chimeric viscometer, featuring a BODIPY–ferrocene motif (Fig. 1 C), exhibited a linear correlation with the viscosity of THF–ethylene glycol mixtures.[49]

Concurrently, the fluorescence lifetimes increased from 2.3 ns to 3.7 ns as the concentration of ethylene glycol increased from 10 to 90%. Furthermore, a triphenylphosphonium-containing coumarin-BODIPY viscometer (Fig. 1 D) was shown to report changes in viscosity within mitochondria.[52] Recently, a chimeric BODIPY-Nile Red probe that is capable of reporting on both polarity and viscosity of the specific media was also developed.[53]

BODIPY dyes are versatile fluorophores whose spectral properties can be tuned via a range of structural modifications.[54, 55] As a result, BODIPY dyes have been explored

in a variety of applications, including molecular, ionic and biological sensing.[56-59] Importantly, BODIPY-based rotors have been shown to be suitable for sensing viscosity, including the viscosity of intracellular environments. Specifically, BODIPY dyes with the modification in the para-position of the phenyl substituent and in the meso- position of the BODIPY scaffold were shown to be viable sensors of intracellular viscosity as their fluorescent lifetime showed a good correlation with viscosity.[44, 45, 60, 61] It should be noted that the so-called ''distorted-BODIPY'' fluorescent viscometer with the carboxyaldehyde-moiety in the meso-position of the BODIPY- scaffold was shown not only to map the viscosity of the cell, but also to detect viscosity changes associated with the early stages of apoptosis in a breast cancer cell line MCF-7.[46] With regard to the BODIPY-based dyads for measuring intracellular viscosity, the coumarin-BODIPY dyad was demonstrated to detect viscosity in mitochondria.[52] In view of the significant linear correlation of both fluorescence intensity and fluorescence lifetimes with viscosity, the aforementioned sensor was shown to be applicable for monitoring viscosity changes that occurred during mitochondrial apoptosis events. Overall, it could be argued that fairly long fluorescence lifetimes (on the order of several ns) along with synthetic accessibility make BODIPY-containing systems a viable platform for the development of fluorescence lifetime based molecular viscometers. It should be pointed out that multistep synthetic protocols that are employed for the preparation of the dyads, BODIPY- based[52] as well as porphyrin-based, which have proven to be very potent in

mapping cellular viscosity[30] should be taken into consideration and they often might be viewed as a draw-back.

In order to overcome this drawback, we decided to explore homodimeric BODIPY dyes, which could be prepared in a few steps from readily available starting materials. Towards this end, we recently assessed the potential of a BODIPY dimer (**BD**) to act as a viscometer for molecular and ionic solvents (Fig. 1.3).[62] Here, we expand on the application of BD and report on its ability to act as a microviscosity sensor in various cellular and membrane-mimicking environments.[63]

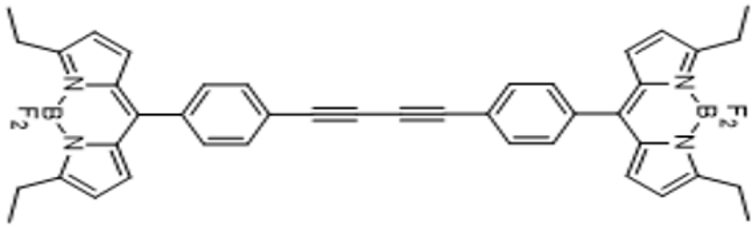

Figure 1.4) Structure of BODIPY dimer (**BD)**

Due to the success of the BODIPY dyad, a BODIPY triad was then synthesized and evaluated. They are composed of a triazine core attached with three BODIPY units, as seen for the rotor in Fig. 1.5. It was synthesized through a three step process, and had an extremely high extinction coefficient, in the 100,000 – 200,000 M^{-1} cm^{-1} range depending on the solvent. The extinction coefficient is a measure of a fluorophore's ability to absorb light, thus relating directly to its sensitivity, *one can use twice less of the BODIPY triad than that of the BODIPY dyad to in a measurement*.

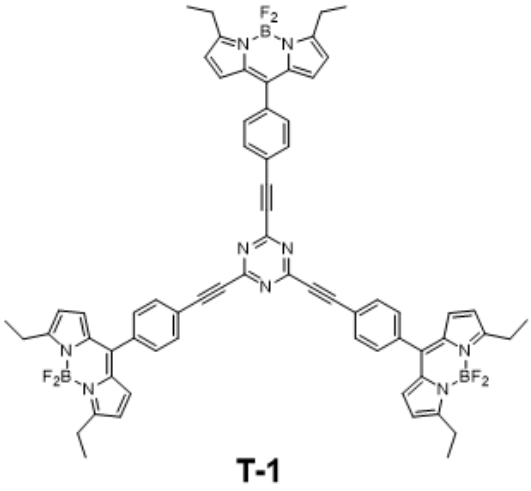

Figure 1.5) Structure of trimeric BODIPY rotor T1

Chapter 2. Theory

2.1 Electronic Transitions

Using a one-dimensional harmonic operator of mass *m* and charge *e* as an approximation to generalize vibrational transitions of molecules which contain electric dipoles, we can explain the process of absorption and subsequently fluorescence.[64] The charged particle will have the potential $V=1/2\ k\ x^2$ in its lowest vibrational state described by the wavefunction Ψ_0 (where k is the spring constant and x is the distance displaced). We need to find a probability that the transition $\Psi_0 \rightarrow \Psi_1$ can be stimulated by light. The total wave function is:

$$\Psi(x,t) = c_0\Psi_0(x,t) + c_1\Psi_1(x,t) \tag{2.1}$$

Where the coefficients c_0 is 1 and $c_1 = 0$ at time zero, thus the oscillator is in its ground state $v=0$ at time zero. Applying a one-dimensional, oscillating electric field, ϵ, will produce a force:

$$F = e\epsilon \tag{2.2}$$

and potential:

$$V = e\epsilon x \tag{2.3}$$

This can then be entered into the time-dependent Schrodinger equation as:

$$\left(\frac{-\hbar^2}{2m}\frac{\partial^2}{\partial x^2}+\frac{1}{2}kx^2+e\epsilon x\right)\Psi(x,t)=i\hbar\frac{\partial\Psi(x,t)}{\partial t} \tag{2.4}$$

Assuming a solution of the form:

$$\Psi=c_0\Psi_0+c_1\Psi_1=c_0\psi_0e^{-iE_0t/\hbar}+c_1\psi_1e^{-iE_1t/\hbar} \tag{2.5}$$

Where E_0 and E_1 are the energies of the two states and c_0 and c_1 are functions of time if the oscillator is to change vibrational states. Inserting (2.5) into the right hand side of (2.4) gives:

$$i\hbar\frac{\partial}{\partial t}\left(c_0\psi_0e^{-iE_0t/\hbar}+c_1\psi_1e^{-iE_1t/\hbar}\right)=i\hbar\left(\Psi_0\frac{dc_0}{dt}+\Psi_1\frac{dc_1}{dt}\right)+c_0\Psi_0E_0+c_1\Psi_1E_1 \tag{2.6}$$

While putting (2.5) into the left hand side of (2.4) gives:

$$\left(\frac{-\hbar^2}{2m}\frac{\partial^2}{\partial x^2}+\frac{1}{2}kx^2+e\epsilon x\right)(c_0\Psi_0+c_1\Psi_1)$$

$$=\left(\frac{-\hbar^2}{2m}\frac{\partial^2}{\partial x^2}+\frac{1}{2}kx^2\right)(c_0\Psi_0+c_1\Psi_1)+e\epsilon x(c_0\Psi_0+c_1\Psi_1)$$

$$=c_0\Psi_0E_0+c_1\Psi_1E_1+e\epsilon x(c_0\Psi_0+c_1\Psi_1) \tag{2.7}$$

Combining and simplifying (2.6) and (2.7) results in:

$$e\epsilon x(c_0\Psi_0+c_1\Psi_1)=i\hbar\left(\Psi_0\frac{dc_0}{dt}+\Psi_1\frac{dc_1}{dt}\right) \tag{2.8}$$

If we multiply (2.8) by Ψ_1^* and integrate over all of space, one gets:

$$\epsilon \int_{-\infty}^{\infty} ex(c_0\Psi_1^*\Psi_0 + c_1\Psi_1^*\Psi_1)dx = i\hbar\left(\frac{dc_0}{dt}\int_{-\infty}^{\infty}\Psi_1^*\Psi_0\,dx + \frac{dc_1}{dt}\int_{-\infty}^{\infty}\Psi_1^*\Psi_1\,dx\right) \qquad (2.9)$$

However, the integral $\int_{-\infty}^{\infty}\Psi_1^*\Psi_0\,dx$ is zero because they are orthogonal wavefunctions, then $\int_{-\infty}^{\infty}\Psi_1^*\Psi_1\,dx$ is equal to unity because the wavefunctions are normalized. Thus we are left with the integral of (9) to be:

$$\epsilon \int_{-\infty}^{\infty} ex(c_0\Psi_1^*\Psi_0 + c_1\Psi_1^*\Psi_1)\,dx = i\hbar\frac{dc_1}{dt} \qquad (2.10)$$

This gives the coefficient for time dependence of the excited state. We can determine how it changes with time when at t=0 when we introduce the electric field. At t=0, c_1=0 and c_0=1, so one can get rid of terms containing c_1 on the left hand side of (2.10). We will use an electric field of

$$\epsilon = \epsilon_0\cos 2\pi\nu t = (1/2)\epsilon_0\left(e^{2\pi i\nu t} + e^{-2\pi i\nu t}\right) \qquad (2.11)$$

For Ψ_0 and Ψ_1 we will use the form from (2.5) and insert these into (2.10) to get:

$$\frac{1}{2}\epsilon_0\left(e^{2\pi i\nu t} + e^{-2\pi i\nu t}\right)\int_{-\infty}^{\infty} ex\psi_1^*\, e^{-iE_1t/\hbar}\psi_0 e^{-iE_0t/\hbar}\,dx = i\hbar\frac{dc_1}{dt}$$

$$\frac{dc_1}{dt} = \frac{\epsilon_0}{2i\hbar}\left(e^{2\pi i\nu t} + e^{-2\pi i\nu t}\right)\left(e^{i(E_1-E_0)t/\hbar}\right)\int_{-\infty}^{\infty} ex\psi_1^*\psi_0\,dx$$

$$\frac{dc_1}{dt} = \frac{\epsilon_0}{2i\hbar}\left(e^{i(E_1-E_0+h\nu)t/\hbar} + e^{i(E_1-E_0-h\nu)t/\hbar}\right)\int_{-\infty}^{\infty} ex\psi_1^*\psi_0\,dx \qquad (2.12)$$

This integral, $\int_{-\infty}^{\infty} ex\psi_1^*\psi_0\, dx$, is the dipole transition moment integral for the transition from the state v=0 to v=1 and can be denoted as μ_{01}. We can integrate (2.12) from t=0 to t to find:

$$c_1 = \frac{\epsilon_0}{2}\mu_{01}\left[\frac{1-e^{i(E_1-E_0+hv)t/\hbar}}{E_1-E_0+hv} + \frac{1-e^{i(E_1-E_0-hv)t/\hbar}}{E_1-E_0-hv}\right] \quad (2.13)$$

We are interested in the case where the energy of the incoming light, hv,[65] approaches E_1-E_0, as this is the requirement for absorption ($\Delta E = hv$). In that case, the 2nd term of (2.13) in brackets approaches zero and thus dominates the 1st term, so we will drop the first term. We are interested in $c_1 * c_1$, as the probability of being in the excited state goes as such. Thus we will multiply (13) by c_1^* to get:

$$c_1 * c_1 = \frac{{\epsilon_0}^2}{4}{\mu_{01}}^2\left[\frac{2-e^{i(E_1-E_0-hv)t/\hbar}-e^{-i(E_1-E_0-hv)t/\hbar}}{(E_1-E_0-hv)^2}\right] \quad (2.14)$$

One can substitute $\sin^2\theta = \frac{1}{4}\left(2 - e^{2i\theta} - e^{-2i\theta}\right)$ which yields:

$$c_1 * c_1 = \frac{{\epsilon_0}^2{\mu_{01}}^2\sin^2[E_1-E_0-hvt/2\hbar]}{(E_1-E_0-hv)^2} \quad (2.15)$$

We need $c_1 * c_1$ valid for all values of incident light (recognizing that only values near the resonance frequency v will give magnitude to $c_1 * c_1$). Thus one can integrate (2.15) from v=0 to ∞ by setting $x = (hv - E_1 + E_0)t\backslash 2\hbar$ and using $\int_{-\infty}^{\infty}\frac{\sin^2 x}{x^2}\, dx = \pi$, so

$$c_1 * c_1 = \frac{{\epsilon_0}^2{\mu_{01}}^2 t}{4\pi\hbar^2}\int_{-\infty}^{\infty}\frac{\sin^2 x}{x^2}\, dx = \frac{{\epsilon_0}^2{\mu_{01}}^2 t}{4\hbar^2} \quad (2.16)$$

And thus we arrive that:

$$\frac{d(c_1 * c_1)}{dt} \propto {\epsilon_0}^2 {\mu_{01}}^2 \tag{2.17}$$

This is a fundamental relationship. At time zero, or the initial rate, at which the excited state is populated is proportional to the square of the amplitude of the electromagnetic radiation, ϵ_0, and the square of the dipole transition moment integral, μ.

For an electronic transition, the transition moment integral is:[66]

$$u = \int \psi'^* \hat{u} \psi \, d\tau \tag{2.18}$$

in which ' stands for the excited state and the dipole moment operator, $\hat{u}$, is then divided into two components:[67] $\hat{u}_n$ which only depends on the nuclear coordinates, and $\hat{u}_e$ which only depends on the electron coordinates. We will define the wavefunction as $\psi = \psi_{es}\psi_n$ then:

$$u = \int \psi^*_{e's'} \psi^*_{v'} (\hat{u}_n + \hat{u}_e) \psi_{es} \psi_v d\tau \tag{2.19}$$

$$= \int \psi^*_{e's'} \psi^*_{v'} \hat{u}_n \psi_{es} \psi_v d\tau + \int \psi^*_{e's'} \psi^*_{v'} \hat{u}_e \psi_{es} \psi_v d\tau$$

$$u = \int \psi^*_{e's'} \psi_{es} \, d\tau_{es} \int \psi^*_{v'} \hat{u}_n \, \psi_v d\tau_n + \int \psi^*_{v'} \psi_v d\tau_n \int \psi^*_{e's'} \, \hat{u}_e \psi_{es} d\tau_{es} \tag{2.20}$$

The integral $\int \psi^*_{e's'} \psi_{es} \, d\tau_{es}$ is zero because the electronic wavefunctions $\psi^*_{e's'}$ and ψ_{es} are orthogonal. The third term, $\int \psi^*_{v'} \psi_v d\tau_n$, is the vibrational term, also known as the Franck-Condon factor. Unlike the first term of the electronic wavefunction going to

zero, the Franck-Condon factor can be non-zero because it is a transition between different electronic states. Furthermore, (2.20) can be written more fully because $\hat{u}_e$ does not act on the spin coordinate as:

$$u = \int \psi_{v'}^{*} \psi_v d\tau_n \int \psi_{e'}^{*} \hat{u}_e \psi_e d\tau_e \int \psi_{s'}^{*} \psi_s d\tau_s \tag{2.21}$$

The square of this formulation gives the probability of a vibrational transition (1st term), electronic orbital transition (2nd term) or a spin transition (3rd term). Thus if any of these are zero, the transition is forbidden, but otherwise gives us a basis for the electronic selection rules in molecules. The Franck-Condon factor essentially gives us the overlap integral of the vibrational wavefunctions in the ground and excited electronic states.

Once a molecule has absorbed this energy, there are a variety of competing processes in which it can it be dissipated and the molecule returned to its ground state. These processes are qualitatively explained in a Jablonski-Perrin Diagram (Fig. 2.1).

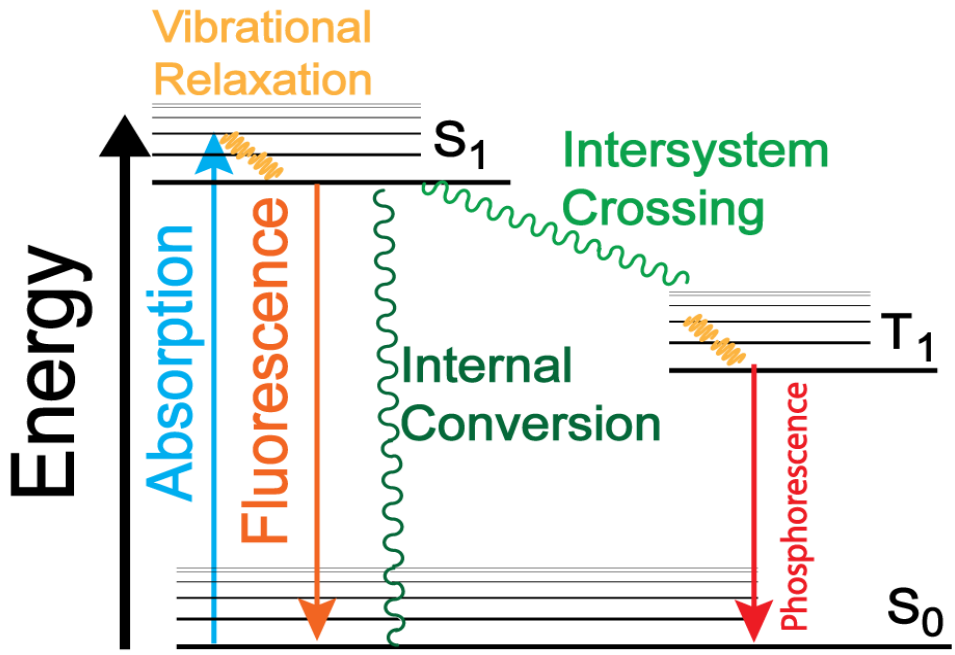

Figure 2.1) Jablonski-Perrin Diagram for possible pathways of the energy absorbed by a molecule. Straight lines involve a photon, wiggly lines do not.

Two different forms are possible, radiative (photon-involved) and non-radiative (photon-less,). We can describe each quantitatively by the rates at which they occur:[68] Γ (radiative) and k_{nr} (non-radiative). The quantum yield of a molecule can be defined as

$$QY = \frac{number\ of\ photons\ emitted}{number\ of\ photons\ absorped} = \frac{\Gamma}{\Gamma + k_{nr}} \tag{2.22}$$

And is typically thought of how effective a molecule is at emitting absorbed light. The ability to emit a photon is governed by the same selection rules discussed above. However, once a molecule has absorbed a photon, the radiative and non-radiative process begin to compete for the energy.

The radiative routes are through fluorescence and phosphorescence (straight lines in Fig. 2.1). In each cause, a photon is released carrying the energy required to

decay to the ground state. Fluorescence occurs when there is no change in spin multiplicity (S_1 to S_0). This is an allowed transition from the 3rd term of (2.21). The time scale for fluorescence is short, on the order of 10^{-9} seconds (nanoseconds). Phosphorescence occurs when there is a change in the spin multiplicity (T_1 to S_0). As this is a spin-forbidden process, the rate is quite slow, on the order of 10^{-4} to 10^{2} seconds.

Non-radiative routes in which energy can be dissipated are through collisions with surrounding molecules (heat), internal conversion (IC) and intersystem crossing (ITC). Internal conversion is the radiationless process of relaxation through vibrational energy levels only with no change in the spin multiplicity. Intersystem crossing is the radiationless transition between electronic states with a change in spin multiplicity. This process is more common in heavy-atom molecules (typically lanthanides) due to their ability to have spin-orbit coupling facilitating the change in spin multiplicity. There are a few other advanced processes, such as Förster energy transfer (FRET) and photochemical reactions, but these are ignored for simplicity here. There is also a non-radiative pathway by intramolecular rotation, or twisting, during the excited state which is associated with a charge transfer, thus a "twisted intramolecular charge transfer" (TICT). This will be discussed further in detail as it is the basis of molecular rotors.

When a photon is emitted, it has lost some amount of energy due to heat dissipation, molecular vibrations, IC or ITC. This energy loss is manifested as the

Stoke's shift, the emitted photon is of less energy than the absorbed photon, as shown for a fluorescein molecule in Fig. 2.2. The absorption transition band is not sharp as one might expect, but somewhat broad as a consequence of the closely spaced vibration energy levels and rotational motion of many (in this case 6 μM fluorescein dye, or 10^{17} molecules) which allows a range of photons to match various transitions.

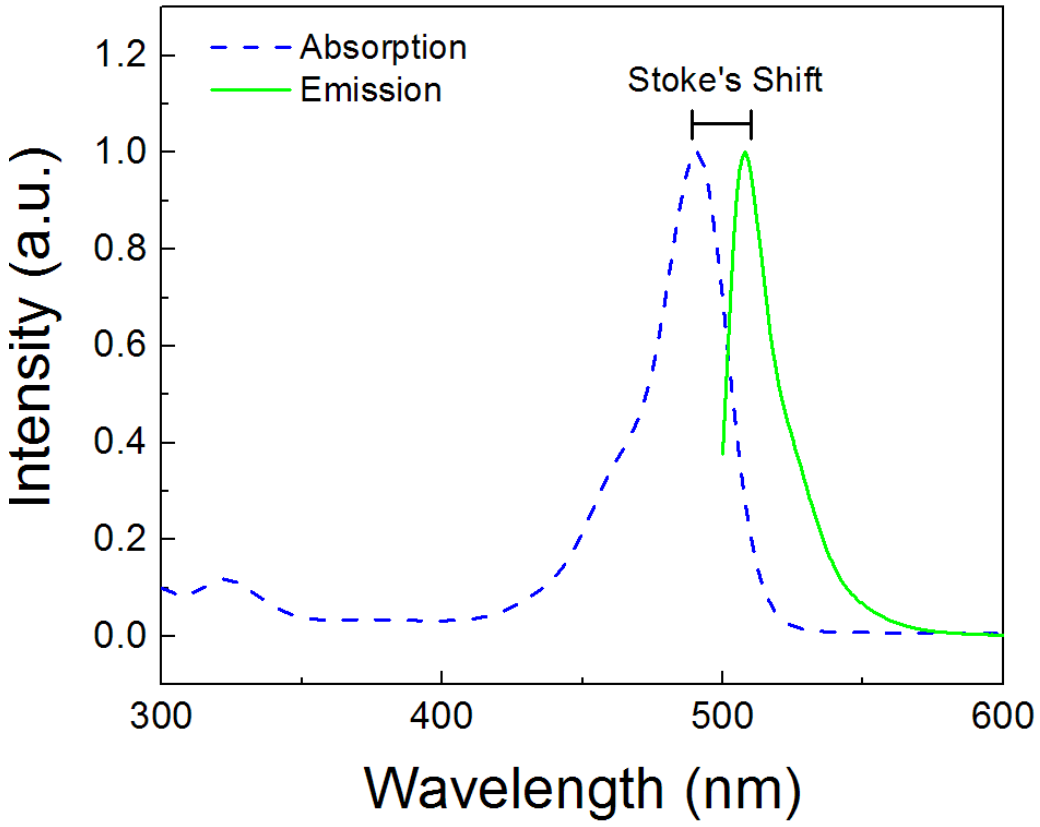

Figure 2.2) Absorption (dotted blue) and emission (solid green) spectra of 6 μM fluorescein

Although absorption can promote the molecule to higher excited electronic states (S_2, S_3, etc.) emission occurs in appreciable amounts only from its lowest excited state of a given multiplicity. This is known as Kasha's Rule, but is a result of the Franck-Condon factor for vibronic transitions. In equation (2.21), we only considered pure electronic

transitions in which ψ_v,and ψ_v were completely symmetric, or 0-0 transitions. In practice, this is not the case, and the electronic and vibrational transitions are coupled and we can rearrange (2.21) as:

$$u = \int \psi_e^*, \psi_v^*, \hat{u}_e \psi_e \psi_v d\tau_n \quad \int \psi_s^*, \psi_s d\tau_s \tag{2.23}$$

In this case, ψ_v,and ψ_v do not have to be completely symmetric for a transition. Thus, radiative transitions could occur from a number of excited electronic energy levels, thus giving off a wide variety of energy photons. However, in the higher excited electronic states, the vibrational energy levels lie much closer to one another. As the greatest overlap integral will occur between vibrationless (v=0) energy levels, these transitions (i.e. $S_3 \rightarrow S_2$), which are actually IC, are coupled greatly and the molecule will reach its lowest excited state (S_1 ,T_1) much sooner than the coupling of higher excited states and the ground state (i.e. $S_3 \rightarrow S_0$). Thus most fluorescence occurs from the first excited electronic state, but there are exceptions. Due to the fact that, typically, the same transitions are involved in both absorption and emission, this leads to the mirror image rule in which the absorption and emission spectra are generally mirror images of each other.

The fluorescence lifetime, or the time spent in the excited state, is the average measurement of all these competing processes:[68]

$$\tau = \frac{1}{\Gamma + k_{nr}} \tag{2.24}$$

If we assume that an initial amount of molecules N_0^* are in the excited state, one can model the amount of molecules in the excited state as a function of time by the first order rate equation:

$$\frac{dN^*(t)}{dt} = -kN_0^*(t) \tag{2.25}$$

Where k is all decay rates (radiative and non-radiative). One can then integrate with respect to time:

$$N^*(t) = N_0^* e^{-kt} \tag{2.26}$$

We can also define the lifetime $\tau = 1/k$ so we are left with

$$N^*(t) = N_0^* e^{-t/\tau} \tag{2.27}$$

Thus the average fluorescence lifetime of a single species is 1/slope for a single component exponential decay, as experimentally shown in Fig. 2.3 for the same 6 μM fluorescein as in Fig. 2.2.

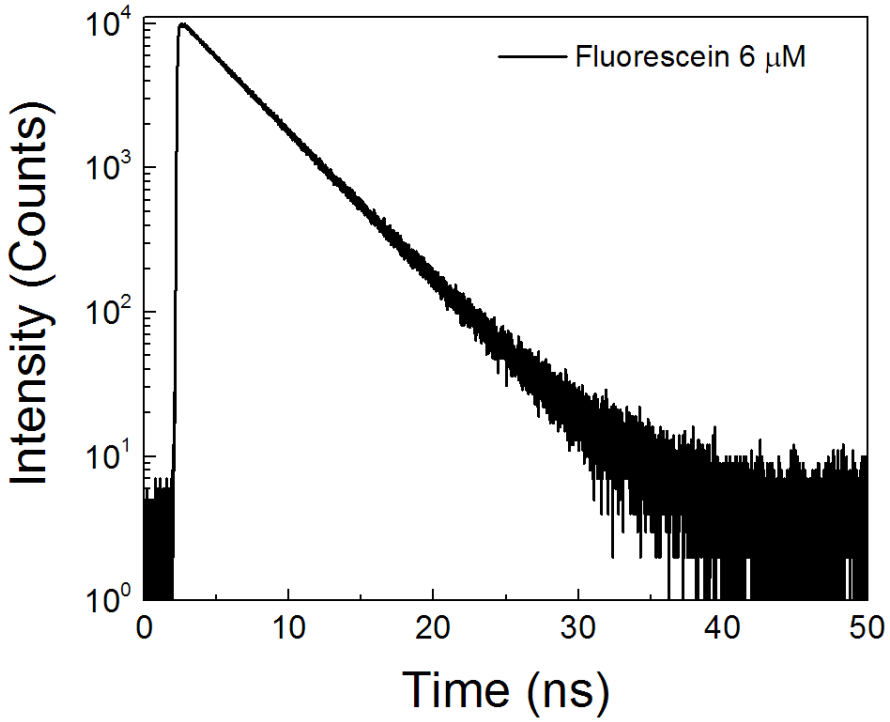

Figure 2.3) Fluorescence intensity decay of 6 μM fluorescein.

This average lifetime is, in general, independent of excitation wavelength, excitation power or concentration. Each species has its own average lifetime, so multiple species can be more easily identified if the lifetime is measured than through steady state methods (absorption, emission, etc). The fact that many typical organic fluorescent molecules have a lifetime in the range of 1-5 ns gives fluorescence spectroscopy an almost unparalled advantage in detection of biological systems because this time range is the time frame in which many biological processes occur. This can also allow the molecule to interact with its environment during the time spent in its excited state.

2.2 Fluorescence Anisotropy

Anisotropy is another tool in which fluorescence can exhibit excellent precision in a wide-range of biomedical studies due to the polarized nature of light. Light travels as an electromagnetic wave. The electric vector can be defined by the plane it travels in, or it's "polarization". Typically, an experiment is run using vertically polarized light to excite the sample, then a polarizer is set on the detection system to measure the intensity of the light parallel ($I_{\parallel}$) or perpendicular ($I_{\perp}$) to the excitation light. The difference in these intensities can be used to measure the fluorescence anisotropy:

$$r = \frac{I_{\parallel} - I_{\perp}}{I_{\parallel} + 2I_{\perp}} \tag{2.28}$$

This difference in emission polarization intensities is due to the fact that a fluorophore's absorption is photosensitive to the polarization of the incoming electric wave. They preferentially absorb photons which their electric vectors are parallel with molecule's transition moment. If the fluorophore emits a photon, it does so along a fixed axis in the molecule, acting as a radiating dipole. If one assumes the excitation and emission transition moments are parallel and with z-axis symmetry (dipole oriented along the z-axis), and no molecular rotation, one can calculate the observed anisotropy for a spherical molecule. First, the electric field created by the molecule is:[68]

$$E(\theta, \phi) = k \frac{\sin\theta}{r} \hat{\theta} \tag{2.29}$$

Where k is a constant, r is the distance to the molecule, θ is the polar angle and ϕ is the azimuthal angle. The intensity of the emitted light is proportional to the square of the electric field:

$$I(\theta, \phi) = k^2 \frac{\sin^2 \theta}{r^2} \hat{r} \tag{2.30}$$

where $\hat{r}$ is a unit vector in the direction of propagation. The projection of the electric field in the z direction is proportional to $\cos\theta$ while along the x-axis it is proportional to $\sin\theta \sin\phi$. Thus the intensities parallel and perpendicular are:

$$I_{\parallel}(\theta, \phi) = \cos^2 \theta \tag{2.31}$$

$$I_{\perp}(\theta, \phi) = \sin^2 \theta \sin^2 \phi \tag{2.32}$$

Next, we must consider randomly oriented fluorophores were excited with the polarized light. For excitation polarized along the z-axis, all molecules at an angle ϕ from the y-axis have equal probability to be excite, or rather put, the fluorophores are symmetrically distributed about the z-axis. The molecules are oriented with values of ϕ from 0 to 2π with equal probability, thus one can drop the ϕ dependence in (2.32).

The average value of $\sin^2 \theta$ from 0 to 2π is ½, so one gets:

$$I_{\parallel}(\theta, \phi) = \cos^2 \theta \tag{2.33}$$

$$I_{\perp}(\theta, \phi) = \frac{1}{2} \sin^2 \theta \tag{2.34}$$

One can assume we observe fluorophores oriented relative to the z-axis at some probability $f(\theta)$. The fluorescence intensity for these molecules is thus:

$$I_{\parallel} = \int_0^{\pi/2} f(\theta) \cos^2 \theta \, d\theta = \langle \cos^2 \theta \rangle \tag{2.35}$$

$$I_{\perp} = \frac{1}{2} \int_0^{\pi/2} f(\theta) \sin^2 \theta \, d\theta = \frac{1}{2} \langle \sin^2 \theta \rangle \tag{2.36}$$

Where $f(\theta)\, d\theta$ is the probability a fluorophore is oriented between θ and $\theta + d\theta$. One can plug (2.33) and (2.34) into (2.28) and reduce to find:

$$r = \frac{3\langle \cos^2 \theta \rangle - 1}{2} \tag{2.37}$$

Thus, the anisotropy is determined by the average value of $\cos^2 \theta$, where θ is the angle between the emission dipole and the z-axis, assuming the fluorophore is symmetric about the z axis. To better understand (2.37), one can see that at θ=0 (co-linear transitions), it gives a value of 1. According to (2.28), this means the measured intensities of the parallel and perpendicular components of emitted light are equal. However, this perfectly oriented system is not possible in a homogenous solution, and the largest value is in fact 0.4.[68] At a value of 54.7°, this results in $r = 0$. This is called the Magic Angle. Thus, one typically measures fluorescence experiments with a vertical polarizer on excitation and one at 54.7° on emission to ensure there is no anisotropy introduced in the measurements.

2.3 Molecular Rotors

Molecular rotors are a subclass of intramolecular charge transfer fluorophores which form a lower energy twisted state.

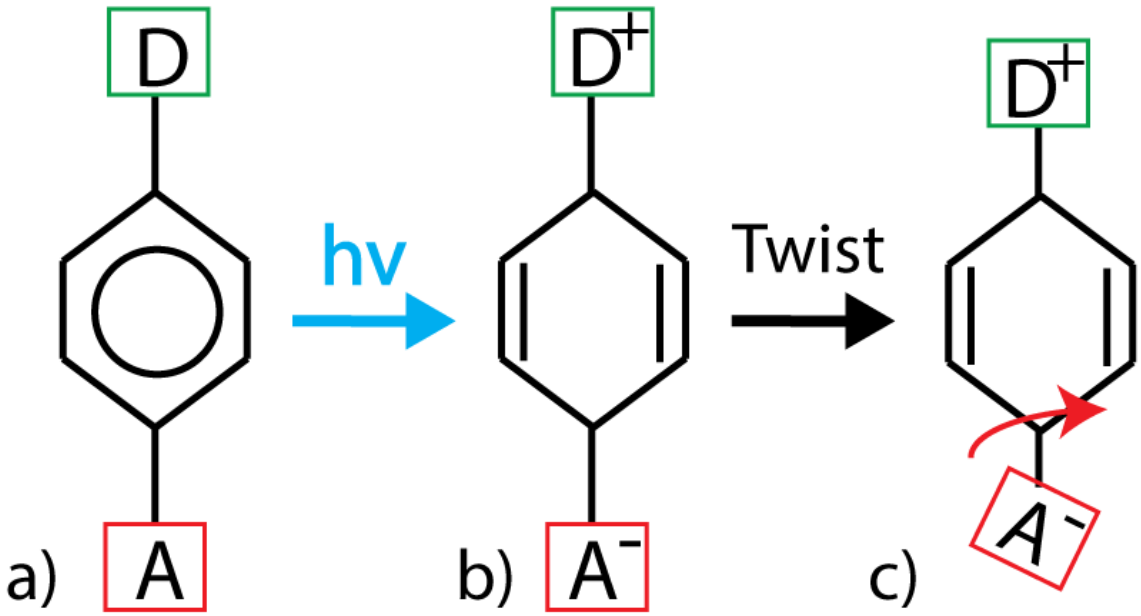

Scheme 2.1) Molecular rotors undergo an intramolecular charge transfer and twist

Typically, an electron donating subunit (D in Scheme 2.1) and an electron acceptor subunit (A in Scheme 2.1) are planar. They are spatially separated, thus limiting, but not eliminating, electron orbital overlap. If the planarity is compromised by even a few degrees, no conjugation is observed. If linked by a single bond, the donor and acceptor subsytems have a limited degree of freedom about the bond. When the moiety absorbs a photon, either the donor or acceptor subunits can be excited (Scheme 2.2, a and b). In both cases, this results in the same charge separated species, $A^{-}\ldots D^{+}$. However, these electrostatic forces now induce a non-planar, twisted, and energetically lower excited

state (Scheme 2.1 c). This process is known as Twisted Intramolecular Charge Transfer (TICT). Occurring in the excited state, these electron transfer reactions are fast, on typically on the order of picoseconds.[69]

Once excited, there are deactivation routes which the excited fluorophore can undergo: radiative[70] and non-radiative.[71] In the case of a radiative decay, the energy is released in the form of a photon and is seen as a shifted band in the emission structure. In this study, this is the case for the porphyrin dimer, **PD**, as seen in Scheme 2.2 c. The twisted state can be formed such that the energy gap is much smaller than the original, planar orientation. In this case, a non-radiative IC process occurs, relaxing the molecule

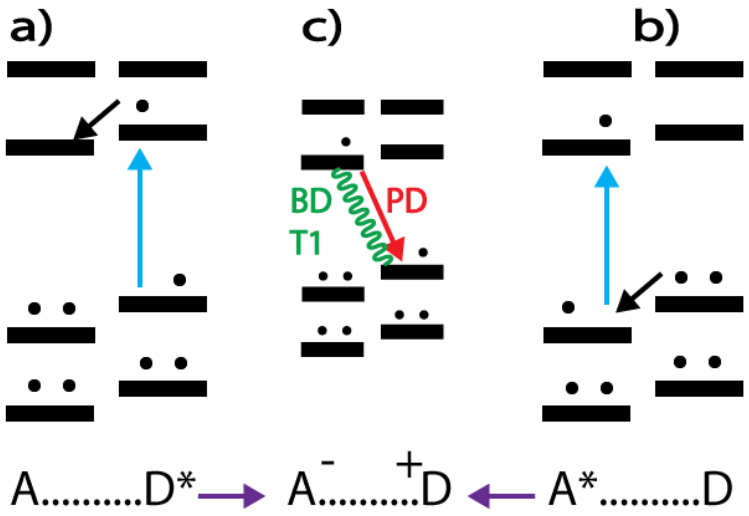

Scheme 2.2) Scheme of photoinduced charge transfer. If either A or D is excited, the same charge state is formed. Energy is released (c) either through a photon (red line, as seen in **PD**) or non-radiative, vibrational decay (green wiggly line, as the case for **BD** and **T1**).

through vibrational means and without a second emission band. This is the case for the BODIPY dyes in this study, **BD** and **T1** in Scheme 2.2 c. They typically display very low

quantum yield in non-viscous solutions, as an increase in viscosity increases the energy barrier to form the TICT state. Solvent polarity can affect some dyes, as ordering charged solutes around the twisting molecule can take energy as well. Thus, the TICT state formation results in a fluorophore which reacts significantly with its surrounding microenvironment.

The fluorescence characteristics of the probe depends on freedom of conformational change. For system where intramolecular conformational change depends on viscosity of the local environment in the proximity of the molecule a linear dependence of the quantum yield and/or fluorescence lifetime as a function of viscosity should be observed. This viscosity dependence of lifetime can be expressed using Förster -Hoffman theory according to the following equation:[72]

$$\log \tau = C + x \log \eta \qquad (2.38)$$

where η is the viscosity, C is the y axis intercept and x is the slope of the line, which is 0.6 for the perfect rotor as predicted by the Förster-Hoffman theory and τ is the fluorescence lifetime of the probe. This equation holds true for the emission quantum yield as well. However, fluorescence lifetime is a much more reliable property than the quantum yield due to its insensitivity to local dye concentration.

Chapter 3. Methodology

3.1 Porphyrin Dimer

All reagents and solvents were from commercial sources (Sigma-Aldrich, Acros, Alfa Aesar) and were used as received. Ionic liquids were synthesized and purified according to literature procedures described below. **PD** was prepared according to literature procedure; the structure and purity were confirmed by MALDI-TOF spectroscopy and HPLC, respectively. A 1 mM concentration stock solution of **PD** in DMSO was prepared fresh prior to experiments, used within 48 h for all spectroscopic measurements, and protected from direct light exposure during storage. All solutions of **PD** in ILs were prepared by addition of the DMSO stock solution to the ionic liquid followed by vortexing at 3,000 rpm for 10-30 seconds.

Absorption spectra were acquired on an Agilent 8453 UV-vis instrument using 1.0 cm quartz cells. The absorption maxima of the Soret band in molecular solvents and their mixtures was centered about 470 nm while for ionic liquids at 475 nm.

Fluorescence measurements were performed using a Shimadzu RF-5301PC as follows: for all molecular solvents and molecular solvent mixtures excitation wavelength was 470 nm; for all ionic liquids excitation wavelength was 475 nm; emission spectra were collected from 600 to 900 nm; excitation and emission slit widths were 3 nm in 1.0 cm quartz cells. All spectra were background subtracted using

appropriate blanks, and subsequently smoothed using manufacturer provided software. Temperature dependent measurements were performed using a Agilent-Cary spectrophotometer with a Peltier temperature controller as follows: λ_{Exc} was 470 nm; emission spectra were collected from 600-900 nm using five scans; excitation and emission slits were 10 nm in a 1.0 cm quartz cell. The samples were equilibrated for 5 min. at a given temperature before the emission spectra were measured. All spectra were background subtracted using the appropriate blanks.

Percent of twisted **PD** conformation (twisted **PD** / %) was calculated as follows:

$$\text{twisted } \mathbf{PD} \text{ / \%} = (F^{max}_{twisted}) \ / \ (F^{max}_{twisted} + F^{max}_{planar}) * 100\ \%$$

where $F^{max}_{twisted}$ is the maximum fluorescence intensity of the twisted conformation; F^{max}_{planar} is the maximum fluorescence intensity of the planar conformation. The maxima were recorded after 5 minutes of allowing the temperature to equilibrate.

Water content of ILs was measured using Aquamax KF coulometric titrator from GRS Scientific according to manufacturer protocols using 0.4 or 0.5 ml of sample. Viscosity and density of ILs were measured using Anton-Paar Lovis 4500M microviscometer. Fluorescence measurements were performed concurrently with the water content measurements.

3.2 Ionic Liquids

All ionic liquids were prepared according to the literature procedures following the general sequences described below.[100] All ionic liquids were purified as follows: ionic liquids were dissolved in CH_2Cl_2, followed by filtration to get rid of inorganic impurities. Next, ionic liquids were repeatedly treated with charcoal in EtOH at elevated temperatures followed by filtration and removal of EtOH in vacuo (for an azeotropic removal of residual water). Finally, the ionic liquids were dried under vacuum for 8-12 hours. All sample preparations and spectroscopic measurements were conducted immediately after removing the ionic liquids from the vacuum with care to minimize the exposure to moisture.

3.3 Spectroscopic Measurements

UV-Vis absorption and fluorescence spectra were obtained using a Cary 50 bio UV–visible Spectrophotometer (Varian Inc.) and Cary Eclipse Spectrofluorometer (Varian Inc.), respectively. All the measurements were done in 0.4mm x 1cm cuvettes with optical density below 0.05, unless mentioned otherwise. In order to measure the quantum yield, absorption spectra of **BD** was collected followed by measuring the integrated fluorescence intensity of the sample. A solution of fluorescein in 0.1M NaOH was used as a reference (quantum yield: 0.90).[73] Fluorescence lifetime was measured on a FluoTime 300 fluorometer (PicoQuant, Inc.) using a 470 nm diode

laser. The fluorometer was equipped with an ultrafast microchannel plate detector (MCP) from Hamamatsu, Inc. The TCSPC was done through a TimeHarp 260 (Picoquant, GmbH) module. The fluorescence lifetimes were measured in the magic angle condition, and appropriate G factors were used to correct for polarization effects. Lifetime data were analyzed using FluoFit4 program from PicoQuant, Inc (Germany) using multi-exponential fitting model:

$$I(t) = \sum_i \alpha_i e^{-t/\tau_i} \quad (3.1)$$

where, αi is the fractional amplitude of the intensity decay of the ith component at time t and τi is the lifetime of the ith component. The intensity and amplitude weighted average lifetimes ($<\tau>_{Int}$, and $<\tau>_{Amp}$) were calculated using the following equations:

$$< \tau >_{Int} = \sum_i f_i \tau_i \quad (3.2)$$

$$< \tau >_{Amp} = \frac{\sum_i \alpha_i \tau_i}{\sum_i \alpha_i} \quad (3.3)$$

$$f_i = \frac{\alpha_i \tau_i}{\sum_i \alpha_i \tau_i} \quad (3.4)$$

Where f_i represents the fractional intensities for each fluorescence lifetime component.

Radiative and non-radiative rates were calculated using experimentally measured quantum yield and fluorescence lifetimes using the following equations:

$$\Phi_f = \frac{k_r}{k_r + k_{nr}} \quad (3.5)$$

and:

$$\tau = \frac{1}{k_r + k_{nr}} \quad (3.66)$$

The (normalized or reduced) χ^2 is the optimization parameter for least squares fitting analysis defined as:

$$\chi^2 = \frac{1}{n-p} \sum_{i=1}^{n} \left[\frac{I_i - I(t_i)}{\sigma_i} \right]^2 \quad (3.7)$$

Where n is the number of data points, p is the number of freely varying parameters, σ_i is the standard deviation, I_i is the measured intensity at time t_i and $I(t_i)$ is the fitted theoretical value for the fitted intensity decay function at time t_i.[74]

3.4 Fluorescence Lifetime Imaging Microscopy (FLIM)

Laser excitation was provided by a pulsed laser diode (PDL-470) emitting a 470 nm light and driven by a PDL 828 ''Sepia II'' driver (Picoquant, GmBH). This driver was operated at 80 MHz. Measurements were performed using a MicroTime 200 time-resolved, confocal microscope from PicoQuant. The excitation and emission light was focused using a 60x 1.2 NA Olympus objective in an Olympus IX71 microscope, and the emission light was filtered using a 488 nm long wave pass filter before passing through a 50 μm pinhole. Detection was made using a hybrid photo- multiplier assembly. The resolution of the time correlated single photon counting (TCSPC) module was set to 4 ps per bin in order to facilitate the detection at the highest possible

resolution. All data analyses were performed using the SymPhoTime software, version 5.3.2. All experimental equipment and the SymPhoTime software were provided by PicoQuant, GmbH, as part of the MicroTime 200 system.

3.5 Cells and Lipids

The SKOV3 (ovarian carcinoma cell), Calu 3 (human epithelial lung cancer) and DU145 (human epithelial prostate cancer) cell lines were obtained from American Type Culture Collection (ATCC), Manassas, VA (USA), and grown to 70% confluence in RPMI supplemented with 10% FBS and 1% Pen-Strep. Cells were trypsinized using 0.25% Trypsin EDTA and seeded on 20 mm round glass-bottom petri dishes. After 24 hours, cells were stained with 500 nM of **BD**/T1 for 20 min at 37 °C. Next, the media was washed 3 times using PBS and fresh PBS was added followed by FLIM imaging on Olympus IX7 microscope.

Four different lipid unilamellar vesicles were prepared using DPPC (1,2-dihexadecanoyl-*sn-glycero*-3-phosphocholine), POPC (1-hexadecanoyl-2-(9Z-octadecenoyl)-*sn-glycero*-3-phosphocholine), POPC + cholesterol and DMPC (1,2-dimyristoyl-*sn-glycero*-3-phosphocholine). Appropriate amounts of each lipid and **BD/T1**were dissolved in chloroform (the lipid : dye ratio was 800 : 1) in glass bottles. The solvent was evaporated under oxygen free nitrogen stream and left overnight to remove any traces of organic solvents. Next, PBS (phosphate buffer saline) was added followed by strong sonication at about 40 °C to get giant multilamellar vesicles.

Moreover, in order to obtain unilamellar vesicles, mutlilamellar vesicles were passed through 100 μm and 0.02 μm membrane syringe filters. As obtained lipid vesicles were used for fluorescence lifetime measurements.

Chapter Four: Results

4.1 Porphyrin Dimer Molecular Rotor

First, the fluorescence spectra of **PD** were measured in ethanol, glycerol and their respective mixtures (Fig. 4.1 A).

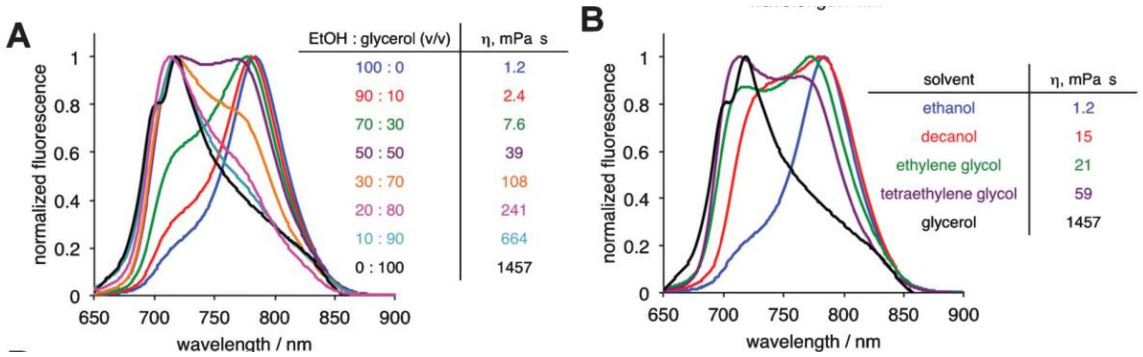

Figure 4.1) Emission spectra of **PD** in A) ethanol/glycerol mixtures; B) various single component solvents

Next, in order to evaluate the scope of single component molecular solvents, the physical properties of more viscous decanol, ethylene glycol and tetraethylene glycol were also measured (Fig. 4.1B).

In order to examine the correlation between the conformational preference of **PD** and the viscosity of ILs, we employed ILs based on one of the most commonly used cationic components, i.e., 1-alkyl-3-methylimidazolium, [C_n-mim]. It is well known that the viscosity of this type of ILs can be altered by varying the length of the alkyl chain as well as the identity of the anion.[75-80] Hence, we prepared

several sets of [C_n-mim]-based ILs (Scheme 4.1) in order to investigate the effect of viscosity on **PD** conformation and potential cation and/or anion effects.

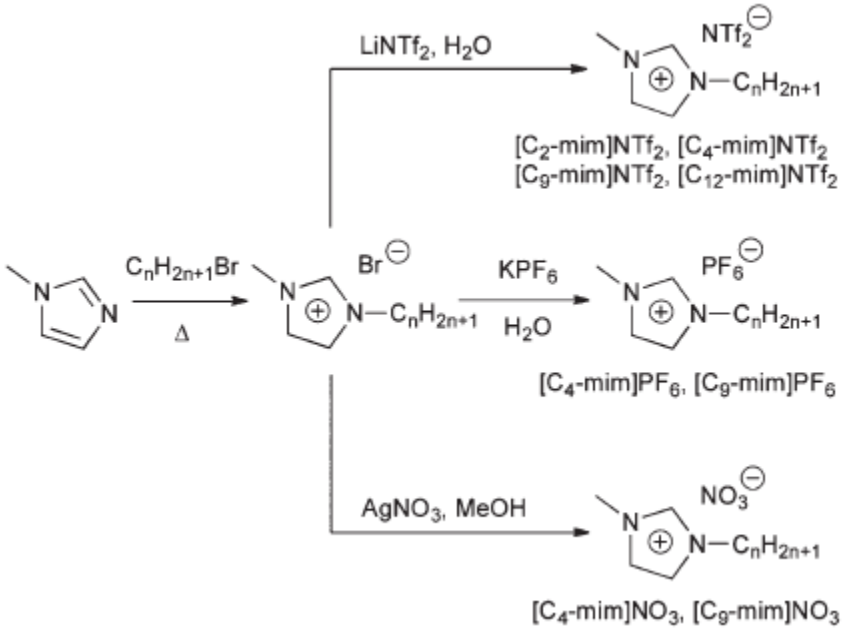

Scheme 4.1) Synthesis and abbreviations of ILs

ILs were chosen to cover a wide range of viscosities.[75-80] In general, for 1-alkyl-3-methylimidazolium-containing ILs, increase of the alkyl chain length leads to more viscous ILs. It is also known that NTf_2-based ILs are among the least viscous imidazolium-type ILs, while viscosity of PF_6-containing ILs spans over a fairly wide range. In addition, NO_3-containing ILs, which are generally much more hydrophilic than the corresponding NTf_2- and PF_6-containing congeners, were chosen due to similarities in viscosity with the PF6-containing set of ILs.[80, 81] Collectively, this set of ILs would aid in identifying possible anion and cation effects on the **PD** conformation.

Entry	Ionic Liquid	Viscosity, mPa•s	Density, g/cm^3	Water content, ppm
1	[C_4-mim]NO_3	262	1.15545	4140
2	[C_9-mim]NO_3	791	1.05085	5473
3	[C_4-mim]PF_6	381	1.37045	347
4	[C_9-mim]PF_6	1324	1.21513	290
5	[C_2-mim]NTf_2	38	1.51923	590
6	[C_4-mim]NTf_2	60	1.43579	469
7	[C_9-mim]NTf_2	116	1.29499	628
8	[C_{12}-mim]NTf_2	202	1.24681	223

a – viscosity and density measurements performed at 20°C.

Table 4.1) Properties of ionic liquids[a]

Furthermore, the viscosity of ILs is known to be greatly affected by the presence of water.[79, 80] Therefore, the water content of all ILs was measured after the viscosity and spectroscopic measurements were performed (Table 4.1). It could be argued that in order for the ILs to be viable from the practical standpoint, all manipulations involving the ILs must be conducted on a bench top. As such, no attempts to reduce the amount of residual water in ILs, beyond commonly applied azeotropic water removal and vacuum drying were taken.

Concurrent with water content measurements, we examined the conformational preference of **PD** in ILs using fluorescence spectroscopy (Fig. 4.2). It should be noted that ILs are intrinsically fluorescent, and the origin of the fluorescence has been debated in the literature.[81] However, a number of experimental and theoretical accounts from various groups have suggested that it is

likely to be related to the microstructuring within ILs.[82] Here, for all fluorescence experiments that feature **PD**, the fluorescence spectra of ILs were subtracted.

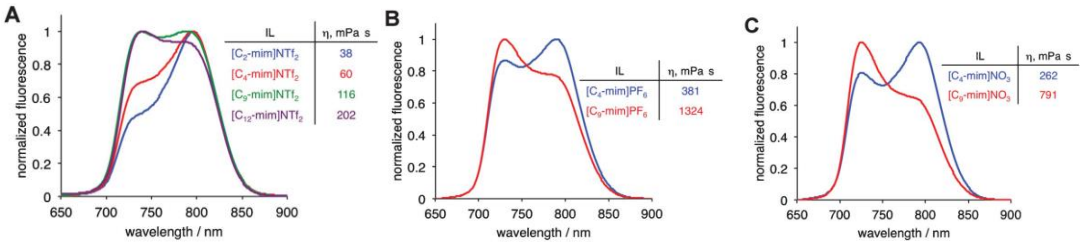

Fig. 4.2 Fluorescence spectra of **PD** in A) [C$_n$-mim]NTf$_2$ ILs; B) [C$_n$-mim]PF$_6$ ILs; C) [C$_n$-mim]NO$_3$ ILs.

4.2 BODIPY Dimer Molecular Rotor

Here, we present a structurally simple and easily accessible symmetric BODIPY–BODIPY dye suitable for probing a wide range of viscosities of both molecular and ionic solvents. Both BODIPY (**1**) and alkyne-BODIPY (**2**) were prepared according to either a conventional synthesis[83] or by a recently developed mechanochemical procedure,[84] and the subsequent dimerization of dye **2** was accomplished under Glaiser-type conditions[85, 86] to furnish **BD** in a moderate yield (Scheme 4.2).

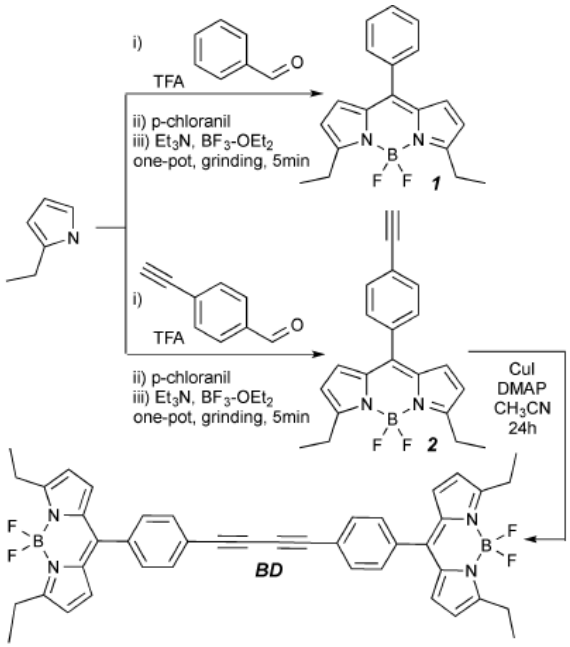

Scheme 4.2) Synthesis of BODIPY based viscometers used in this work: dye **1**, dye **2** and **BD**.

The fluorescence spectra of dyes **1**, **2**, and **BD** in ethanol, propylene glycol, and glycerol revealed that the position of neither the absorption nor the emission maxima (Table 4.2) were greatly affected by the viscosity of the media

DYE	SOLVENT	λ_{abs} / nm	λ_{ex} / nm	$\langle\tau\rangle_{int}$ / ns	$\langle\tau\rangle_{amp}$ / ns	Φ
1	ethanol	510	523	1.390	1.250	0.19
	propylene glycol	511	524	2.870	2.500	0.35
	glycerol	513	525	4.610	4.610	0.80
2	ethanol	512	529	0.550	0.290	0.04
	propylene glycol	515	530	0.870	0.810	0.13
	glycerol	515	525	3.060	2.820	0.48
BD	ethanol	512	532	0.326	0.223	0.04
	propylene glycol	513	532	1.463	1.344	0.19
	glycerol	516	533	4.500	4.155	0.48

Table 4.2) Photophysical properties of dyes **1, 2** and **BD** in molecular solvents at 20 ° C.

SOLVENT	T / °C	Viscosity / mPa•s
ethanol (1985 ppm)[a]	5	1.8
	20	1.4
	35	1.0
	50	0.8
propylene glycol (1100 ppm)[a]	5	198
	20	70
	35	30
	50	15
glycerol (970 ppm)[a]	5	ND[b]
	20	1475
	35	506
	50	181

a – water content as determined by KF titration at room temperature;

b – not determined; m.p. of glycerol 17.8°C.

Table 4.3) Effect of temperature on the viscosity of molecular solvents.

On the other hand, the lifetime of dyes **2** and **BD** appeared to change notably (Table 4.2). Specifically, the fluorescence intensity decay times for dye **2** increased from $\langle\tau\rangle_{Int}$ = 0.550 ns in ethanol (η = 1.2 mPa s) to $\langle\tau\rangle_{Int}$ = 3.060 ns in glycerol (η = 1457 mPa s). In the case of **BD**, the change was even more pronounced with $\langle\tau\rangle_{Int}$ = 0.326 ns in ethanol as compared to $\langle\tau\rangle_{Int}$ = 4.500 ns in glycerol. Although dye **1** showed only a marginal (*ca*. 3-fold) increase in the fluorescent lifetime within the given viscosity range (Table 4.3), this change is worth noting, primarily in view of a very simple structure of **1**, where the rotor was realized by a simple rotation of the phenyl group in the meso-position. Owing to the large change in fluorescence lifetime over the given viscosity range (1.2 to 1457 mPa s), i.e., 13.8-fold for **BD** as compared to 5.6-fold for **2**, and 3.3-fold for **1**,

we chose to further explore the possibility of using **BD** as a potential molecular viscometer.

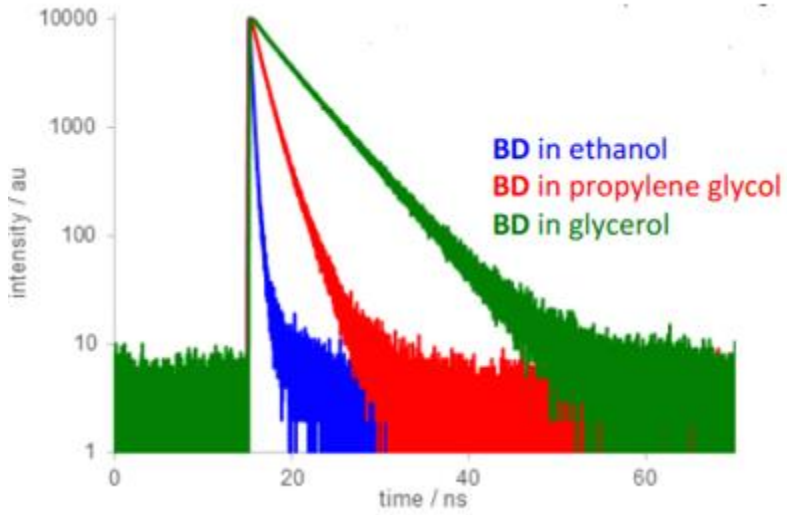

Figure 4.3) Fluorescence intensity decays of **BD** in molecular solvents at 20 °C

SOLVENT	T / °C	τ_1 / ns	τ_2 / ns	τ_3 / ns	α_1	α_2	α_3	$\langle\tau\rangle_{int}$	$\langle\tau\rangle_{amp}$	χ^2
EtOH	5	2.461	0.500	0.210	0.0022	0.1523	0.8455	0.343	0.262	0.95
	20	3.796	0.470	0.190	0.0012	0.1083	0.8905	0.326	0.223	0.97
	35	4.096	0.410	0.155	0.0012	0.0748	0.9240	0.303	0.178	0.95
	50	3.993	0.433	0.134	0.0012	0.0316	0.9672	0.287	0.148	0.99
Propylene glycol	5	3.514	2.087	-	0.1717	0.8283	-	2.456	2.332	0.95
	20	2.224	1.163	-	0.1714	0.8286	-	1.463	1.344	0.96
	35	1.759	0.719	-	0.0751	0.9249	-	0.891	0.797	1.03
	50	2.156	0.476	-	0.0160	0.9840	-	0.591	0.503	0.97
Glycerol	5	5.288	2.081	-	0.8366	0.1634	-	5.059	4.764	0.99
	20	4.701	1.573	-	0.8282	0.1718	-	4.500	4.155	0.99
	35	4.049	2.00	-	0.6439	0.3561	-	3.610	3.321	1.04
	50	4.045	1.848	-	0.2343	0.7657	-	2.729	2.363	1.02

Table 4.4) Effect of temperature of fluorescence lifetime of **BD** in molecular solvents.

Next, in order to explore other types of environments, we decided to probe the potential of BD as a molecular viscometer in ionic media, i.e., room-temperature ILs, and 1,3-dialkylmidazolium ILs are among the most widely used and studied ILs.[11] These solvents have found numerous applications, and they could be viewed as customizable materials since their physical properties, including viscosity, can be tuned via structural modifications of the cationic and anionic counterparts.[11, 87-89] The viscosity of the 1-alkyl-3-methylimidazolium ILs can be modulated over a wide range by simply adjusting the length of the alkyl chains, as well as the identity of the anion.[79, 90-93]

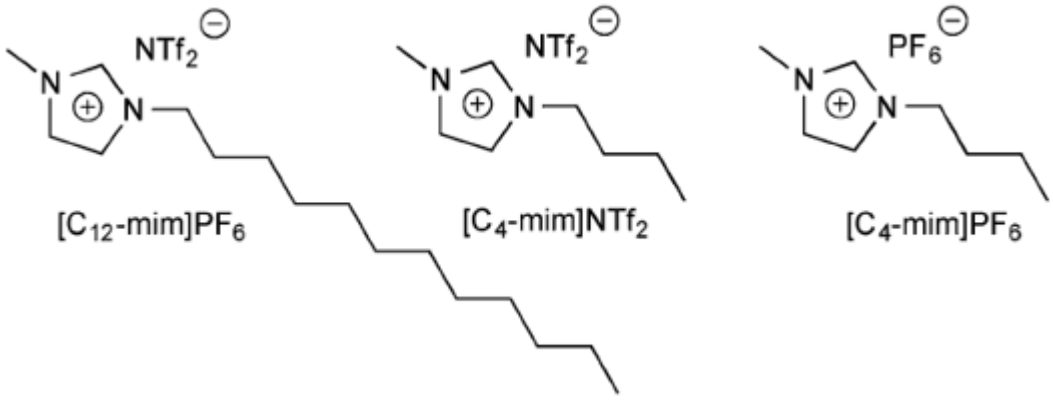

Figure 4.4) Structures of Ils used in this work.

Importantly, on the structural level, neat ILs could be viewed as heterogeneous, supramolecular polymer-like assemblies (or nanostructured domains) as opposed to molecular solvents that are homogeneous fluids.[82, 94-98] This heterogeneity was also demonstrated to be crucial in controlling the outcome of several organic reactions performed in ILs.[99, 100]

Here, we investigated the behavior of **BD** in several ILs, namely [C4-mim]PF_4, [C4-mim]NTf_2, and [C12-mim]NTf_2 (Fig. 4.4). These ILs were chosen based on (i) their broad viscosity range (78 to 435 mPa s at 20 ° C, see Table 4.5), which complements that of the molecular solvents (Table 4.3), and (ii) their largely non-hygroscopic nature (as compared to more hydrophilic ILs, such as NO_3- and BF_4-containing ILs). This was expected to facilitate the handling and manipulation of the ILs during the measurements.

IONIC LIQUID	Temperature / °C	Viscosity / mPa•s
[C_4-mim]PF_6 (1720 ppm)[a]	5	1307
	10	880
	20	435
	30	234
	35	179
	40	139
	50	89
	60	61
[C_4-mim]NTf_2 (707 ppm)[a]	5	169
	10	129
	20	78
	30	51
	35	44
	40	36
	50	27
	60	21
[C_{12}-mim]NTf_2 (430 ppm)[a]	5	729
	10	516
	20	248
	30	144
	35	116
	40	97
	50	66
	60	47

a – water content as determined by KF titration at room temperature.

Table 4.5) Effect of temperature on viscosity of ionic liquids.

DYE	SOLVENT	λ_{abs} / nm	λ_{ex} / nm	$\langle\tau\rangle_{int}$ / ns	$\langle\tau\rangle_{amp}$ / ns	Φ
BD	$[C_4\text{-mim}]PF_6$	514	533	2.244	2.101	0.29
	$[C_4\text{-mim}]NTf_2$	514	533	1.384	1.260	0.22
	$[C_{12}\text{-mim}]NTf_2$	516	536	2.276	1.906	0.48

Table 4.6) Photophysical properties of **BD** in ionic liquids at 20 ° C

Similar to molecular solvents the absorption and emission spectra of **BD** were virtually unchanged in all three ILs (Table 4.6), while the fluorescent lifetimes of **BD** increased as the viscosity of the ILs increased (Fig. 4.5 and Table 4.6). In addition, multi-exponential fluorescence decays were noted for **BD** as well (Table 4.4).

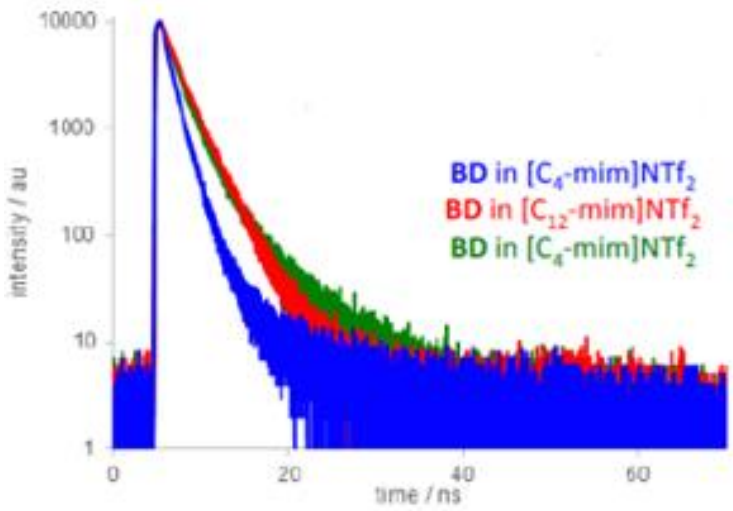

Figure 4.5) Fluorescent intensity decays for **BD** in ionic liquids at 20 ° C

4.3 BODIPY Dimer Application

Our goal was to establish whether a simple BODIPY homodimer could act as a molecular rotor, with its fluorescence emission and the fluorescence lifetime being sensitive to the ambient viscosity. It appeared that changing the viscosity of the media (by using ethanol: glycerol mixtures[101]) did not significantly affect the shape and peak emission wavelength (Fig.

4.6). A small shift of the emission maximum (~7 nm) was observed when viscosity changed from that of ethanol to that of glycerol and this could be ascribed to slight changes in the media polarity.

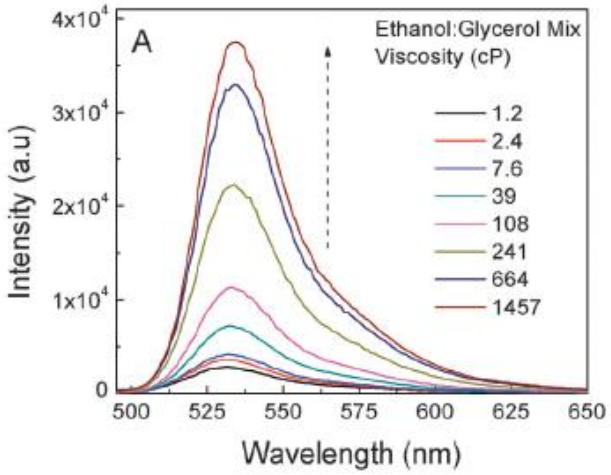

Figure 4.6) Emission spectra of the **BD** in different visocisy mixtures of ethanol:glycerol

Additionally, increasing the viscosity of the media increased the emission intensity and fluorescence quantum yield, which is consistent with Equation (2.38).

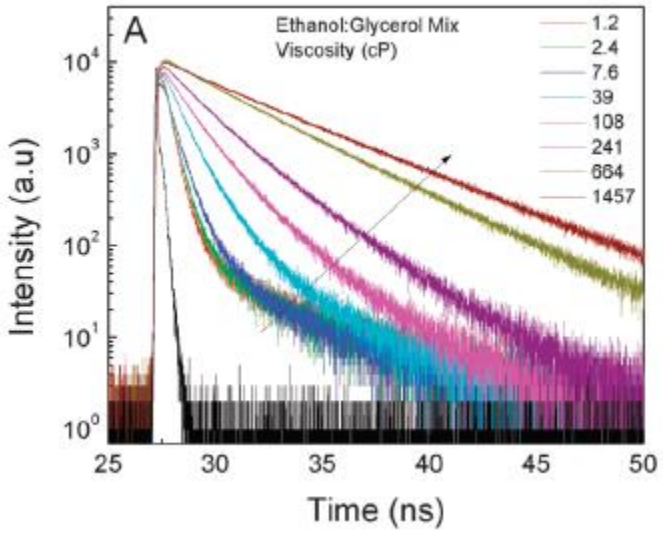

Figure 4.7) Fluorescence intensity decays of **BD** in different viscosity mixtures of ethanol: glycerol

Fluorescence intensity decays at increasing viscosity in ethanol: glycerol mixtures were measured (Fig. 4.7) and the fluorescence lifetime changed distinctly as a function of viscosity.

Prior to the cellular studies, we envisioned that investigations using simple lipid vesicles would be advantageous for further understanding of the cellular observations. Thus, encapsulation of the **BD** into vesicles, which were made from different lipid components and physical states, could give an idea about the possible position of the dye molecules in lipid bilayers and their surrounding microviscosity from fluorescence lifetime measurements. Thus, the lifetime data of **BD** in DPPC, POPC, and POPC + cholesterol were evaluated (Table 4.7).

Lipid Vesicles	τ_{AMP} / ns	τ_{INT} / ns	Viscosity /cP
DPPC	1.30	1.93	200
POPC	1.54	2.07	220
POPC+cholesterol	1.62	2.20	260

Table 4.7) Average fluorescence lifetimes of **BD** obtained in different lipid vesicles and the corresponding viscosities calculated.

We envisioned that using the fluorescence lifetime versus viscosity calibration plots obtained in ethanol: glycerol mixtures (Fig. 5.8) would allow us to determine the viscosity distribution in cells via FLIM. Even though the fluorescence lifetime of a fluorophore could be influenced by several environmental parameters apart from viscosity, such as refractive index, polarity, pH, or chemical and physical quenching processes, it was shown that BODIPY dyes were insensitive to changes in such environmental parameters and can be unambiguously used to probe the intracellular viscosity.[61, 102]

The **BD** was readily taken up by the SKOV3 cells. A bright punctate distribution of the dye was observed throughout the cells. Moreover, very low intensity regions in cytosols were also present. We expected the **BD** to target the hydrophobic membrane regions owing to its hydrophobic nature as seen from the lipid vesicle experiments. Punctate distribution appeared to be due to the accumulation of the dye in certain cell organelle membranes (Fig. 4.8 A). This distribution pattern was found to be similar to the one observed by Levitt *et al*.[61] the difference being less intense cytosolic fluorescence in our case. The lifetime distribution of the dye was examined after 20 min. of incubation time. Furthermore, with longer dye incubation time (1 h), no significant differences in distribution of the **BD** inside cells was observed. It is possible that the dye uptake mechanism might be a passive diffusion since the endocytotic uptake is energy dependent, yet the exact dye uptake mechanism remains to be clarified.

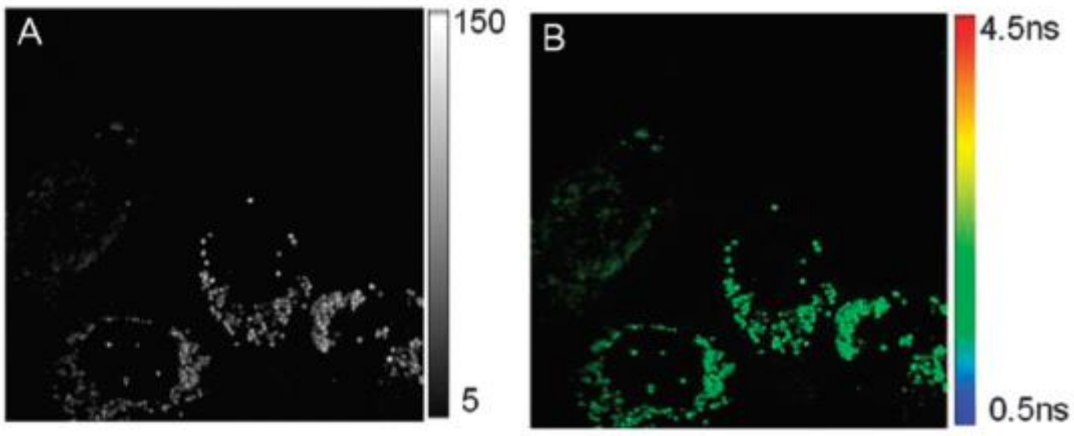

Figure 4.8) A) Confocal intensity image (80x80 μm) of SKOV3 cells treated with **BD** B) FLIM image of SKOV3 cells treated with **BD**

Following the calibration of fluorescence lifetimes of the **BD** as a function of viscosity, we performed FLIM analysis to generate a spatial map of viscosity in SKOV3 cells incubated with the **BD** (Fig. 4.8 B).

The initial observation of the dye distribution indicated that these organelles could be either mitochondria or lysosomes. Thus we decided to carry out the co-localization experiment using respective fluorescent markers and the **BD** (Fig. 4.9).

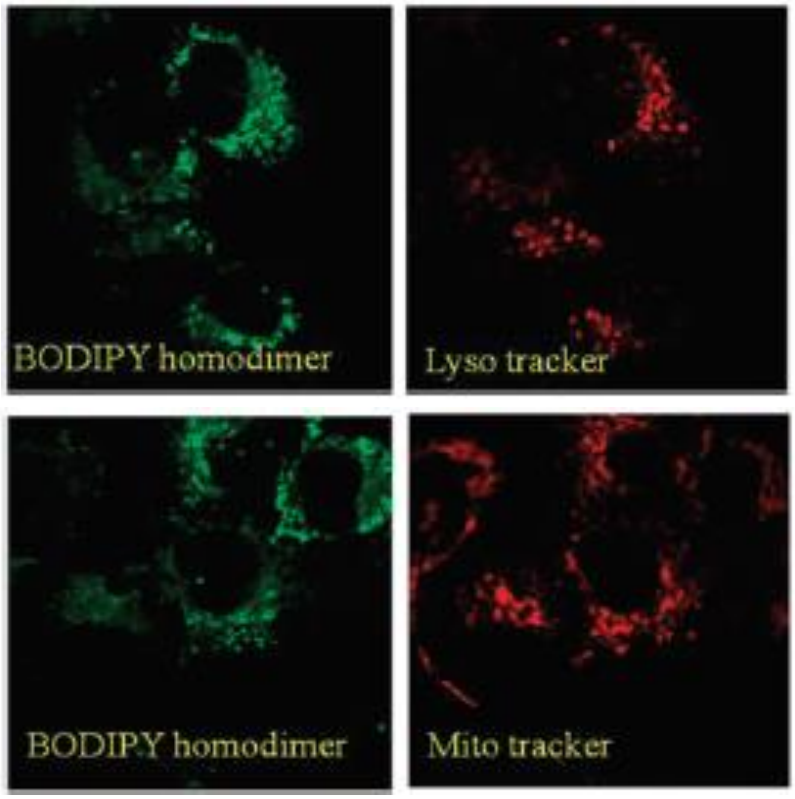

Figure 4.9) SKOV3 cells treated with **BD** and Lysotracker (top) and Mitotracker (bottom)

4.3 BODIPY Trimer Molecular Rotor

Here, we report on a novel, easily accessible fluorescent trimeric BODIPY dyes **T1** and **T2** (Scheme 4.3) with extinction coefficients in the range of 200,000 M^{-1} cm^{-1}

(Table 4.8). Dye **T1** can act as a small molecule viscometer for molecular solvents as well as cellular and membrane-like environments. Dye **T2** has methyl substitutions at the 1 and 7 positions that hinder the molecular rotation limiting the conformational change. In effect, the fluorescence signal change is small and can be interpreted as simple solvent effects.

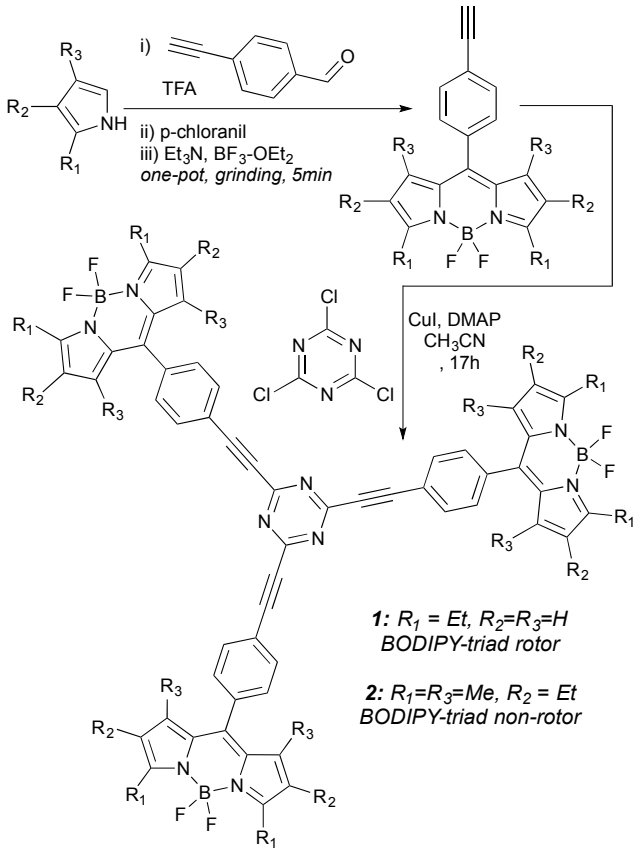

Scheme 4.3) Synthesis of BODIPY trimers **T1** (rotor) and **T2** (non-rotor)

SOLVENT	ε / M^{-1} cm^{-1}	
	T1	T2
ethanol	206000	235000
glycerol	99000	99000
ethanol/glycerol – 90/10 (v/v)	189000	232000
ethanol/glycerol – 50/50 (v/v)	193000	325000
ethanol/glycerol – 10/90 (v/v)	92000	75000
1,2-dichloroethane	174000	242000
dimethylsulfoxide	150000	216000
PBS buffer, pH 7.4	62000	99000

Table 4.8) Extinction coefficient of dyes **T1** and **T2** in various solvents

In this study, we took advantage of the three reactive chlorines of the triazine to assemble three BODIPY dyes to synthesize BODIPY trimers (Scheme 4.3). Specifically, alkyene-containing BODIPY dyes were prepared according to published procedures[62], and subsequent cross-coupling reactions furnished the BODIPY trimers **T1** (rotor) and **T2** (non-rotor) in just two steps from commercially available starting materials.

Excitation and emission spectra of rotor and non-rotor dyes (in ethanol 1: λ_{Exc}= 516 nm, λ_{Ems} = 535 nm; 2 = λ_{Exc} = 528 nm, λ_{Ems} = 540 nm) indicated that there is a small redshift, arguably attributed to the alkyl substitutions on the BODIPY core (Figure 4.10).

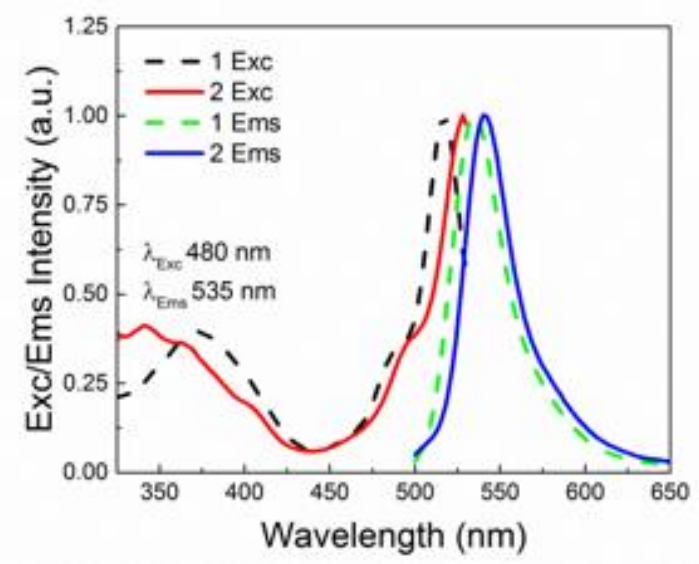

Figure 4.10) Excitation and Emission spectra of **T1** and **T2**.

The methyl groups in the positions 1 and 7 on the BODIPY backbone prevent the rotation about the phenyl group during excitation, thus making it insensitive to its surrounding viscosity changes. However, when these methyl groups are absent (in the case of dye **T1**), this rotation is possible. This then suppresses the non-radiative decay pathways, thus making the molecule sensitive to its surrounding viscosity. Dye **T2** can be used to correct the emission intensity or lifetimes measured of dye **T1** in order to eliminate the changes due to other factors (e.g. polarity) than viscosity.

Furthermore, we examined how the emission of **T1** and **T2** depended on the viscosity of the media (Fig. 4.11). Samples of different viscosities were prepared by mixing the appropriate amounts of ethanol and glycerol[101]. Emission intensity increased *ca*. 12 times as viscosity increased from 1.2 cP (ethanol) to 1457 cP (glycerol) in a linear manner, as expected for any molecular rotor based on the Förster -Hoffman theory. In

addition, quantum yield changed by *ca*. 12 fold (Fig. 4.11 inset). A less than a two-fold change in emission intensity was observed for non-rotor **T2** in the same range of viscosity, while the quantum yield (0.60) remained unchanged.

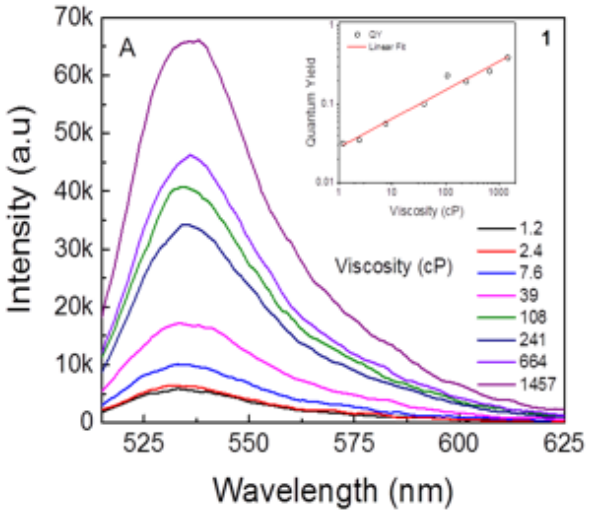

Figure 4.11) Emission spectra of **T1** in ethanol: glycerol mixtures, insert shows quantum yield vs. viscosity.

Moreover, steady state emission anisotropy was also evaluated as a function of viscosity for both **T1** and **T2** (Fig. 4.12). Emission anisotropy of **T1** in ethanol was found to be around 0.1 and in glycerol it increased to 0.25. On the other hand, the anisotropy of **T2**, i.e., the non-rotor dye, in ethanol was found to be close to zero, yet in in glycerol, the anisotropy was found to be ca. 0.25, i.e., similar to that observed for the rotor **T1** at high viscosity.

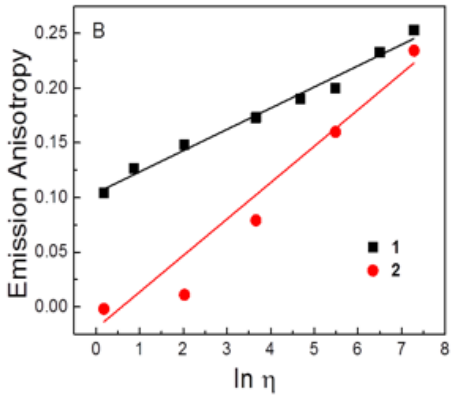

Figure 4.12) Emission Anisotropy of **T1** and **T2** vs. log viscosity in various ethanol: glycerol mixtures.

Absorption and emission spectra of **T1 (**Fig. 4.13 top) and **T2** (Fig. 4.13 bottom) were also recorded in solvents with varying polarities.

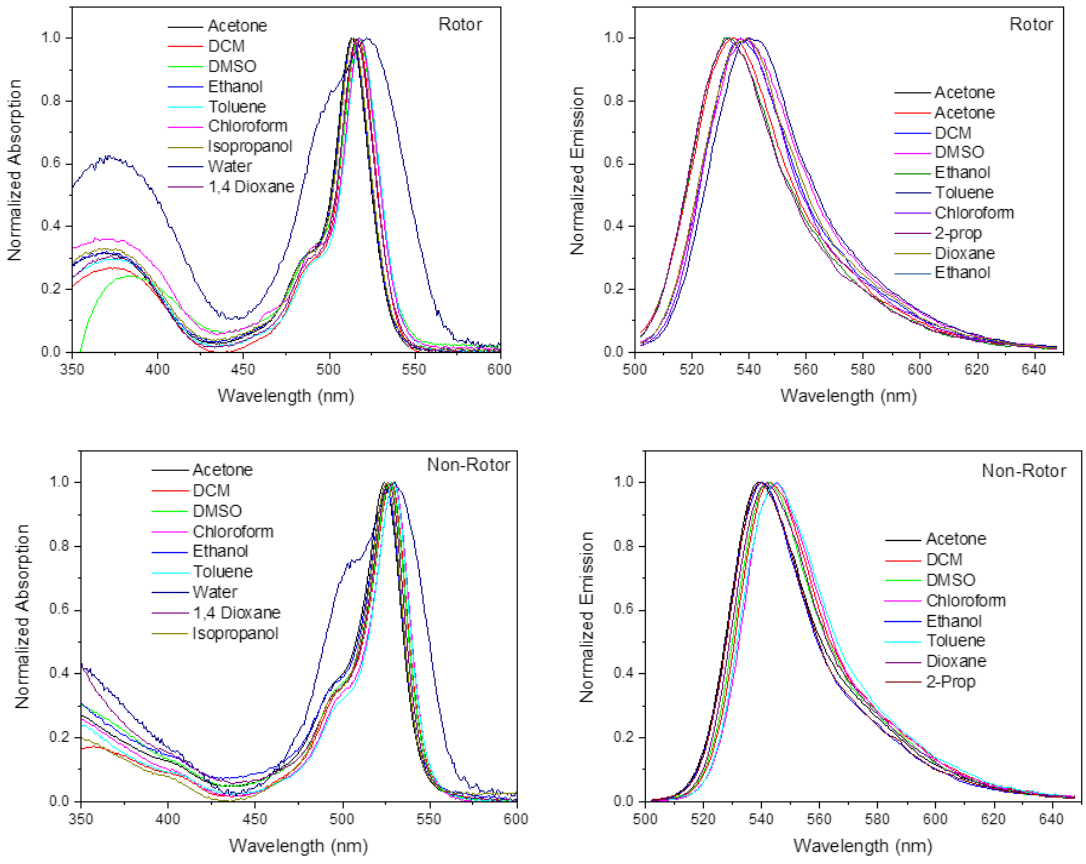

Figure 4.13) Normalized absorption and emission spectra of **T1** (top) and **T2** (bottom) in various polarity solvents.

As previously mentioned, quantum yield and intensity are not reliable parameters for measuring viscosity due to their dependence on the local dye concentration, for example. Thus, we examined the fluorescence lifetimes of the **T1** in different viscosities (Fig. 4.14). As expected, the fluorescence intensity decays of **T2** were virtually independent of viscosity (Fig. 4.14- only 3 traces are shown due to strong overlap of the intermediate decays).

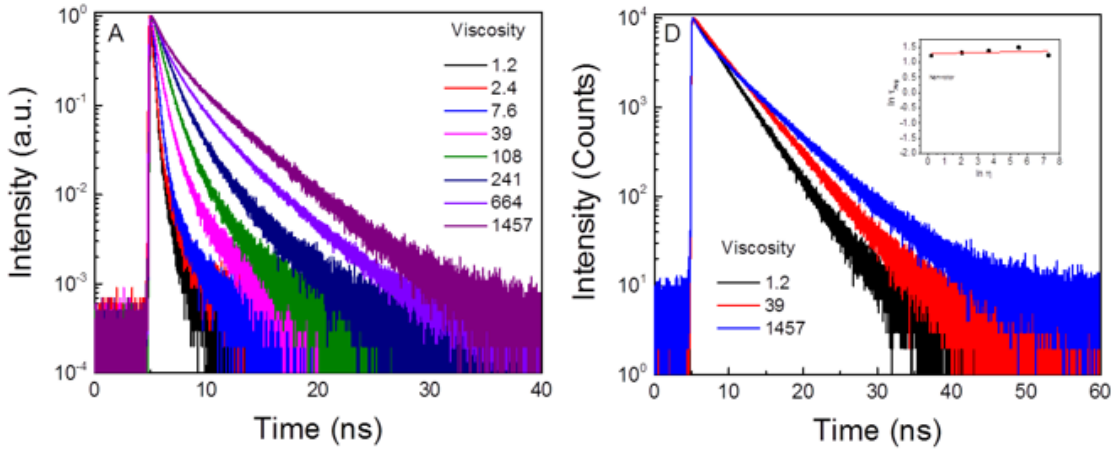

Figure 4.14) Fluorescence intensity decays of **T1 (**left) and **T2** (right) in various ethanol: glycerol mixtures.

Next, we encapsulated **T1** and **T2** in DMPC lipid vesicles and measured their fluorescence lifetimes (Fig. 4.15) at various temperatures (15, 23 and 30 ^{o}C).

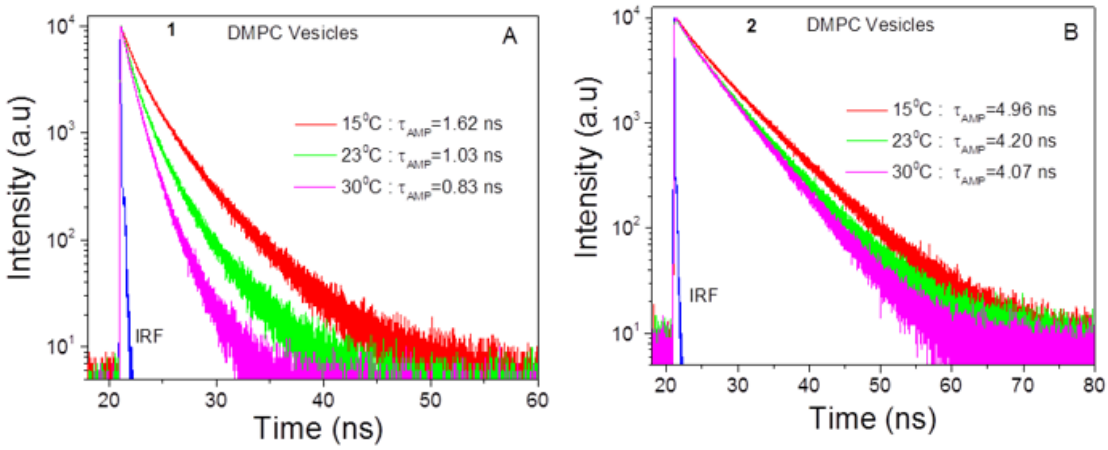

Figure 4.15) Fluorescence intensity decays of **T1** (A) and **T2** (B) in DMPC vesicles at various temperatures.

Further, we investigated the cellular distribution of **T1** with the aim of measuring the intracellular viscosity. Towards this end, the behavior of rotor **T1** was tested in two different cancer cell lines (Fig. 4.16): Calu 3 (adenocarcinoma of the lung) and DU 145 (a prostate cancer) through FLIM.

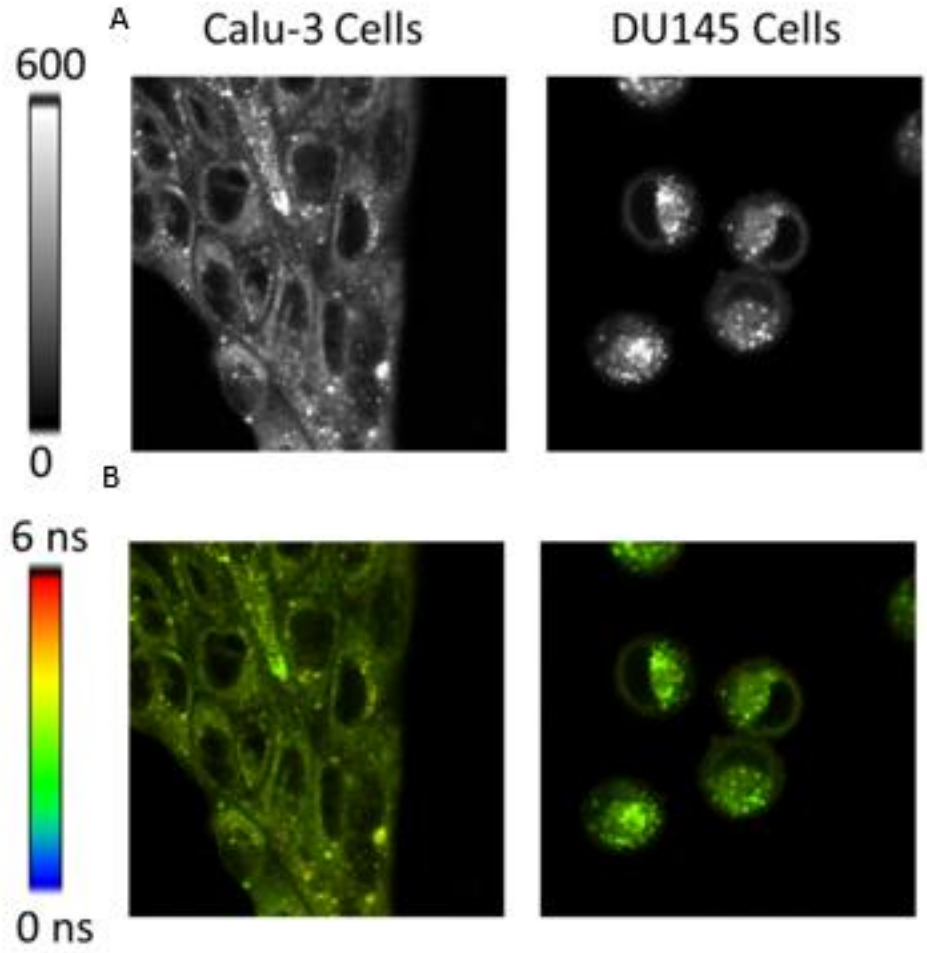

Figure 4.16) (**A**) 80x80 μm intensity images of Calu3 (left) and DU145 cells (right) treated with 500 nM of **T1** (**B**) 80x80 μm FLIM images of Calu 3 (left) and DU 145 (right) cells treated with 500 nM **T1.**

Chapter 5: Discussion

5.1 Porphyrin Dimer

Qualitatively our results were in complete agreement with the published data:[30] the planar conformer of **PD** dominated in less viscous media, whereas the twisted conformation started to dominate in more viscous media. Specifically, the switch from the planar to the twisted conformation of **PD** took place at a molecular solvent viscosity of *ca.* 39 mPa s. *Notably, a good linear correlation between the viscosity and a conformational preference of **PD** was found* (Fig. 5.1). This is indicative of a molecular rotor with TICT and a radiative decay route.

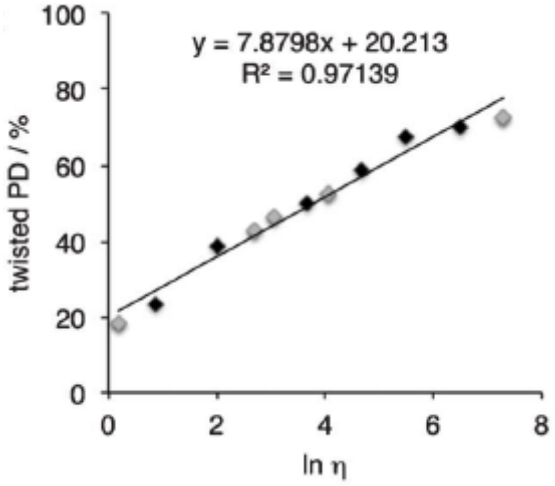

Figure 5.1) Effect of media's viscosity on % of twisted **PD**: black diamonds – EtOH-glycerol mixtures, grey diamonds- single component solvents.

Viscosities of common imidazolium-based ILs are known to be orders of magnitude higher than those of many common molecular solvents, and as such the twisted conformation of **PD** was expected to be seen for all ILs with a

viscosity of *ca.* 40 mPa s. However, in contrast to molecular solvents (Fig. 4.1 A,B), IL [C_2- mim]NTf_2, with η = 38 mPa s significantly promoted the planar conformer of **PD** (Fig. 4.2 A). As the viscosity of the NTf_2-containing ILs increased as a function of the alkyl chain length, the preference for the twisted conformation of **PD** increased as well. A similar effect was observed for the PF_6- and NO_3-containing ILs (Fig. 4.2 B and 4.2 C, respectively). Thus, the cation of the ILs might have a significant role in the conformational bias of **PD**.

Furthermore, when the viscosity was plotted as a function of the twisted conformation of **PD**, an apparent correlation was observed (Fig. 5.2), albeit the linearity was found to be somewhat poorer from that observed in the case of the molecular solvents (Fig. 5.1).

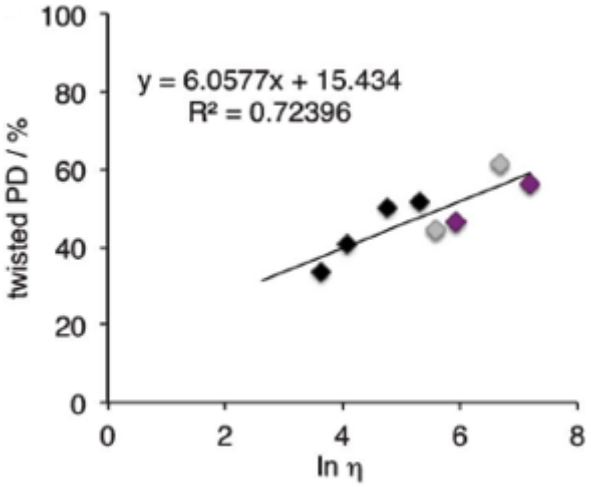

Figure 5.2) Effect of IL's viscosity on % of twisted **PD**: [C_n-mim]NTf_2 – black symbols; [C_n-mim]PF_6 – purple symbols; [C_n-mim]NO_3 – grey symbols.

In addition, since the slope in the case of ILs is smaller than that compared to molecular solvents, i.e., 6.0577 versus 7.8798, respectively, a significantly higher viscosity would be required for ILs to induce the twisted conformation when compared to the molecular solvents. Overall, within each set of ILs with a common anion, the percentage of the planar conformation of **PD** appeared to decrease as the viscosity of the IL increased (Fig. 4.2). For example, in all [C4-mim]-containing ILs (Fig. 3), despite *ca.* 6-fold viscosity range (60 for [C_4-mim]NTf_2 to 262 for [C_4-mim]NO_3 to 381 mPa s for [C_4-mim]PF_6), the planar conformation of **PD** was observed (although a linear correlation with viscosity was noted). This was reminiscent of the correlation with viscosity observed in the molecular solvents (Fig. 5.1).

However, upon closer examination of the aforementioned trend (Fig. 5.2), it is evident that the *viscosity of the ILs might not be a dominant factor in controlling the conformational bias of **PD**.* Specifically, when comparing the viscosities of [C_{12}-mim]NTf_2, [C_4- mim]NO_3 and [C_4-mim]PF_6, which progressively increased in viscosity from 202 to 262 to 381 mPa s, no correlation in regard to the **PD** conformation was observed. An inverse correlation was evident for [C_9-mim]NO_3 and [C_9-mim]PF_6 ILs (Fig. 5.2) with increasing viscosity of IL, the planar conformation started to dominate.

It is plausible that in ILs specific solvent–solute interactions (as well as the structure of ILs) could control the conformation of a small molecule, rather than the viscosity of the media. Unlike molecular solvents, which interact with solutes via dipole–dipole interactions and hydrogen bonding, ILs have the added ability to interact via ion–, and ion–ion interactions, i.e., via electrostatic interactions. It was also suggested that a significant amount of solute stabilization by ILs comes from the cation,[82] which might explain the apparent cation effect observed here.

To gain further support for the notion that viscosity of ILs might not be the dominant factor in controlling **PD**'s conformation in ILs, we examined the relationship between viscosity and conformational bias of **PD** as a function of temperature. Arguably, if the viscosity were the main factor that modulated the conformation of **PD**, then changing the temperature (and as a result changing the viscosity of the solvent) should result in a linear correlation between the viscosity and the percent of the twisted conformation of **PD**. Also, the slope should be similar to that observed for solvents of various viscosities at a fixed temperature. Conversely, if the slope of the viscosity (obtained at different temperatures) as a function of **PD** conformation would be different from the slope obtained for solvents of various viscosities at a fixed temperature, some specific interactions between the solvents and **PD** might be present.

To test this hypothesis, we examined the conformation of **PD** in several molecular solvents and ILs at various temperatures and consequently viscosities (Fig. 5.3). The slope of viscosity as a function of the twisted **PD** in EtOH–glycerol (2: 8 v/v) mixture as well as tetraethylene glycol (Fig. 5.3 A). Arguably, this indicated that the viscosity of molecular solvents was the major factor that controlled the conformational bias of **PD**.

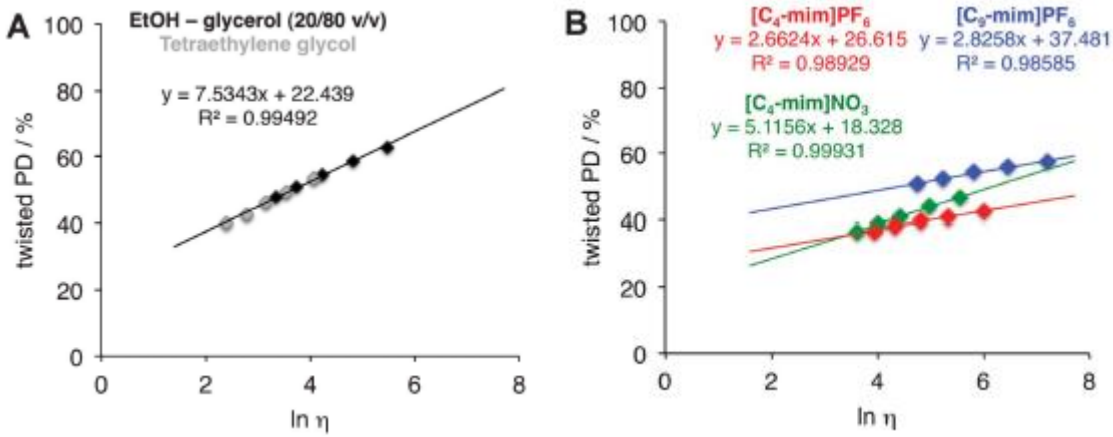

Figure 5.3) Effect of solvent (A: molecular solvents; B: ILs) viscosity on % twisted **PD** measured at 20-60 ° C to control the viscosity from 0.8 to 1475 cP.

On the contrary, in ILs no apparent correlation among several different ILs was observed (Fig. 5.3 B). Although for PF_6-containing ILs ([C_4-mim]PF_6 and [C_9-mim]PF_6) somewhat similar slopes were obtained, the two data sets were off-set. When the ILs with the same cation were compared ([C_4-mim]NO_3 and [C_4-mim]PF_6), the corresponding slopes were found be distinctly different. Therefore, it is plausible that in ILs, solute–solvent specific interactions are playing a significantly more

prominent role than viscosity. This is in contrast to the observation noted for the molecular solvents.

Finally, we decided to investigate the effect of water in $[C_4$- mim$]NO_3$ ILs on the viscosity of the IL as well as the conformational preference of **PD**. Following the aforementioned rationale on the effect of temperature on viscosity and the conformation of **PD**, we reasoned that the presence of water should alter the **PD**–$[C_4$-mim$]NO_3$ interactions, which should produce a distinct correlation between IL viscosity and **PD** conformation from that observed upon variation of temperature (Fig. 5.3 B) as well as the structure of ILs (Fig. 5.2). It is worth pointing out that in water alone, **PD** was found to be non-fluorescent.[103] Consistent with this assumption, we observed a linear correlation between the viscosity of $[C_4$-mim$]NO_3$ with various amounts of water and the conformation of **PD** (Fig. 5.4). However, the slope was found to be drastically different, i.e., 7.7892 as compared to 5.1156, from that found for the temperature effect of the **PD** emission in $[C_4$-mim$]NO_3$ (Fig. 5.3 B), for example.

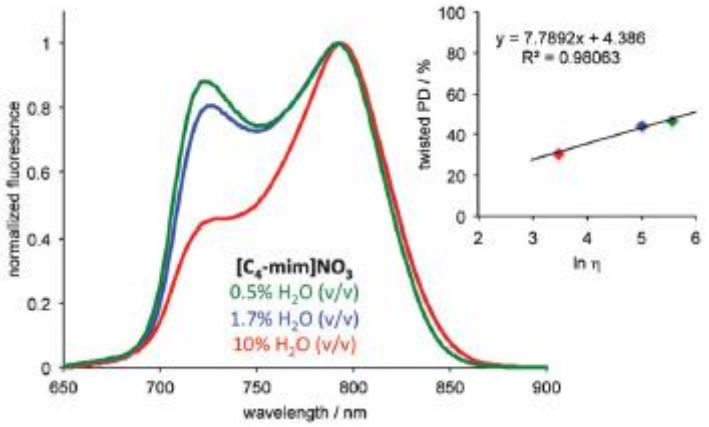

Figure 5.4) Emission spectra of **PD** in [C_4-mim]NO_3 as a function of the water content. Insert: effect of [C_4-mim]NO_3 viscosity (red symbol-10% of H_2O, blue symbol- 1.7% of H_2O and green- 0.5% of H_2O) as a function of **PD** conformation.

Overall, the structure of ILs appeared to have an effect on the conformation of **PD**. ILs promoted the opposite conformation as molecular solvents with similar viscosities, i.e., planar vs. twisted, respectively, and an order of magnitude larger viscosity of ILs was required to promote a similar amount of twisted **PD**. Specifically, the viscosity range at which twisted conformation becomes dominant is shifted from *ca.* 40 (in molecular solvents) to 400 (in ILs) mPa s range. There appeared to be linear correlations between **PD's** conformation and the viscosity in ILs, molecular solvent mixtures and single component molecular solvents.

However, the cation effect (in all ILs with a common cation a similar conformation of **PD** was present, regardless of viscosity) seemed to indicate that the structure of IL could control the conformation of **PD**. In this light, it is important to distinguish between properties of ILs that correlate with a given process and those

that actually control the process. Hence, in ILs with short alkyl chain lengths i.e. [C_4-mim] and [C_2-mim], the solvent–solute interactions promoted the planar conformation, regardless of viscosity. Similarly, ILs with longer alkyl chains, i.e., [C_9-mim] and [C_{12}-mim], seemed to promote the twisted conformation, which happened to correlate with the increased viscosity of the solvent. *However, it was apparent that the structure of ILs plays a more important role in the control of the* ***PD*** *conformation and the correlation between the ILs' viscosity, and* ***PD*** *conformation might be coincidental*. It should be noted that a microheterogenous nature of the ILs could be playing a role as well.[104, 105]

While the exact nature of the observed phenomena remains to be elucidated, this report highlighted the designer solvent ability of ILs in that ILs of different structures gave rise to different **PD** conformations. Notably, an order of magnitude higher viscosity was required in ILs to induce a similar conformation of **PD**, potentially emphasizing specific interactions between the ILs and **PD**.

5.2 BODIPY Dimer Molecular Rotor

Furthermore, the effect of media's temperature on the fluorescence lifetime of **BD** was studied in ethanol, propylene glycol, and glycerol (Table 4.2 and Table 4.3) and showed an apparent linear correlation between the viscosity

of the solvents and the fluorescence lifetime of **BD** (Fig. 5.5). This observed correlation between the fluorescent lifetimes and the viscosity of the media (which is changed by both altering the nature of the media and/or altering the temperature of the media) should be indicative of the fact that viscosity is indeed the main factor that modulates the conformation preference of **BD**. This is indicative of a molecular rotor which undergoes TICT with a non-radiative decay route. It should also be pointed out that the fluorescence intensity decays exhibited a multi-exponential behavior as a function of the identity of the solvent as well as temperature (Table 4.2). *Collectively, these results suggested that **BD** could potentially be used as a simple, minimalistic dyad to monitor viscosity of the molecular media.*

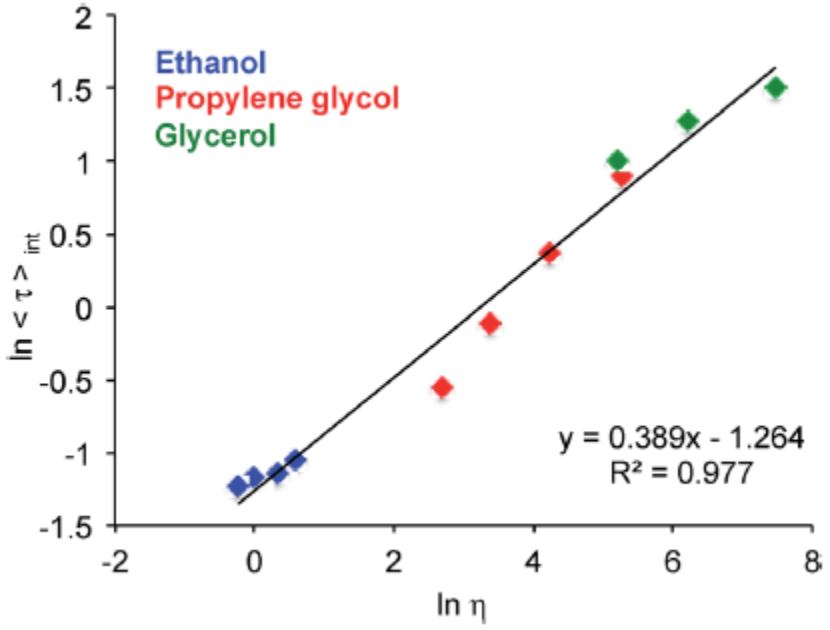

Figure 5.5) Effect of media's viscosity on the lifetime of **BD** in ethanol, propylene glycol and glycerol in a 5-50 ° C (ΔT = 15 ° C) temperature range.

However, when the fluorescence lifetimes of **BD** in ILs were plotted as a function of ILs' viscosity, a dramatically different relationship from that observed in molecular solvents (Fig 5.5) was observed (Fig. 5.6). Specifically, for the two ILs with the same cation, i.e., [C_4-mim]PF_6 and [C_4-mim]NTf_2, the slopes were 0.498 and 0.696, respectively, whereas for the ILs with the same anion, i.e., [C_4-mim]NTf_2 and [C_{12}-mim]NTf_2 the slopes were 0.696 and 0.249, respectively (Fig. 5.6). *It could be argued that a different slope in the viscosity versus lifetime dependence is attributed to a unique solute–solvent interaction.*

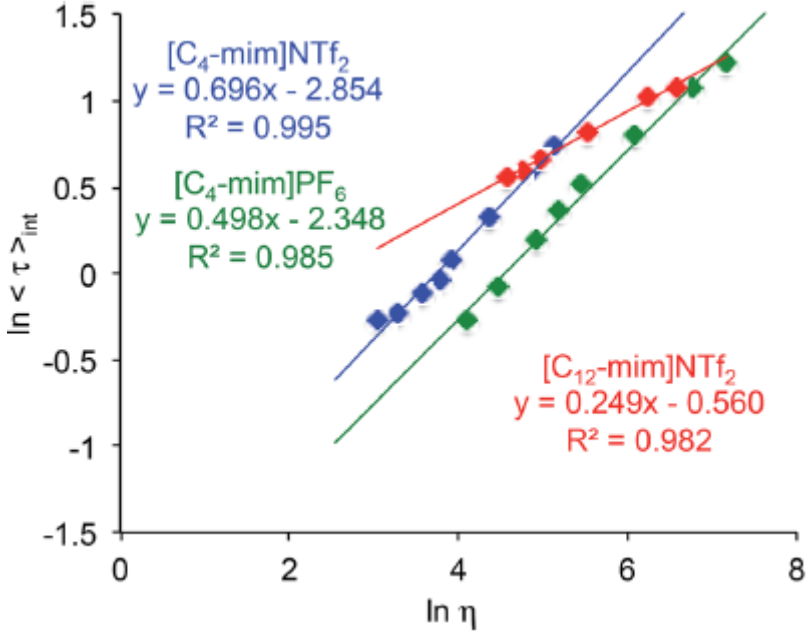

Figure 5.6) Effect of media's viscosity on the lifetime of **BD** in ionic liquids in a 5-60 ° C (ΔT = 10 ° C) temperature range.

Alternatively, it could also be proposed that unique behavior of **BD** in each IL might be due to distinct nanostructured assemblies of these ILs. Considering that in molecular solvents i.e., ethanol, propylene glycol, and glycerol, within a

similar temperature range (5–60 °C), a linear correlation for all solvents was observed (Fig. 5.5), which could indicate that no specific interactions between the solvent and **BD** exist and/or no heterogeneous domains exist in these solvents.

It is also worth noting that the spectroscopic behavior of an ionic porphyrin-based viscometer in molecular solvents was quite different from that in ILs.[101] Although these results suggested that generalizations regarding the viscosity of ILs using molecular viscometers should be carried out with caution, due to the unique nature of this type of media, it might be possible, in principle, to use such molecules to probe the nature of heterogeneous IL domains and/or assess how different the IL domains could be (in terms of the heterogeneity).

The assessment of the viscosity of ILs using **BD** was less straightforward than in molecular solvents, most likely due to specific solvent interactions and/or the unique aggregation state (or heterogeneity) of specific ILs. [106]

5.3 BODIPY Dimer Application

The value of Φ_f, as a function of viscosity in ethanol: glycerol mixtures, is shown in Fig. 5.7. Linear dependence of viscosity with regard to the Φ_f of the BODIPY dimer was observed for viscosities above 20 cP.

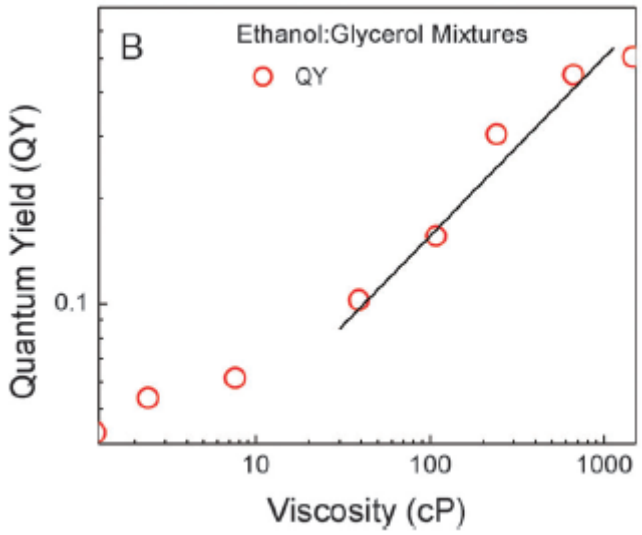

Figure 5.7) log-log plot of **BD** quantum yield and viscosity.

The fluorescence lifetime dependence was similar to quantum yield, a linear dependence was observed for media's viscosity above 20 cP (Fig. 5.8). Specifically, the fluorescence lifetime in ethanol (1.2 cP) was 340 ps, while in glycerol (1457 cP) the lifetime increased to 4.3 ns.

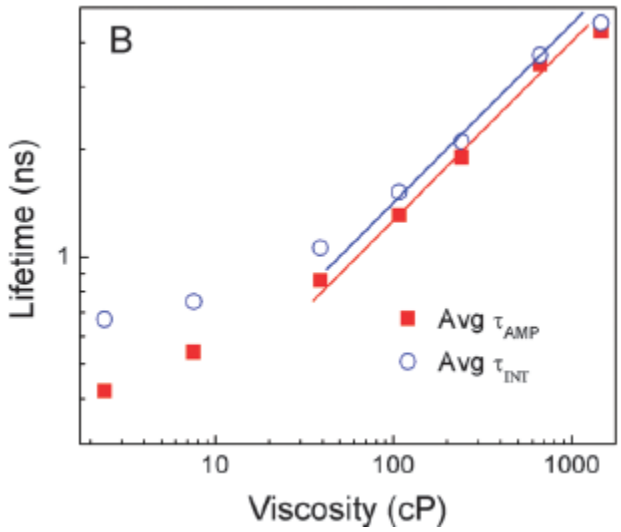

Figure 5.8) Average fluorescence lifetimes as a function of viscosity.

The fluorescence lifetimes at viscosities between 1.2 and 1457 cP were all above 300 ps. This is important, since the lower limit for lifetime resolution of our TSCPC (most of time-resolved systems available today) is significantly below 300 ps. Considering Equation (2.38), it was expected that the plot should have produced a linear dependence between the lifetime and log-viscosity. *Indeed, this was confirmed at viscosities above 20 cP, giving a slope of 0.46.* This value compared well with the value of 2/3 predicted by Forster and Hoffmann[72]. Typical slope values range from 0.2 to 1.4 for different rotors[107]. We found that below 20 cP, the fluorescence lifetime and quantum yield were minimally variant. Arguably, the viscosity dependent rotational resistance for BODIPY units in the dimer became insignificant at lower viscosities.

The rate constants, K_r and K_{nr}, were calculated from the experimentally measured quantum yields and the fluorescence lifetime using Equations 2.22 and 2.24. In ethanol, quantum

yield was 0.02 and it increased significantly as the viscosity of the solution increased, as expected based on Equation (2.38).

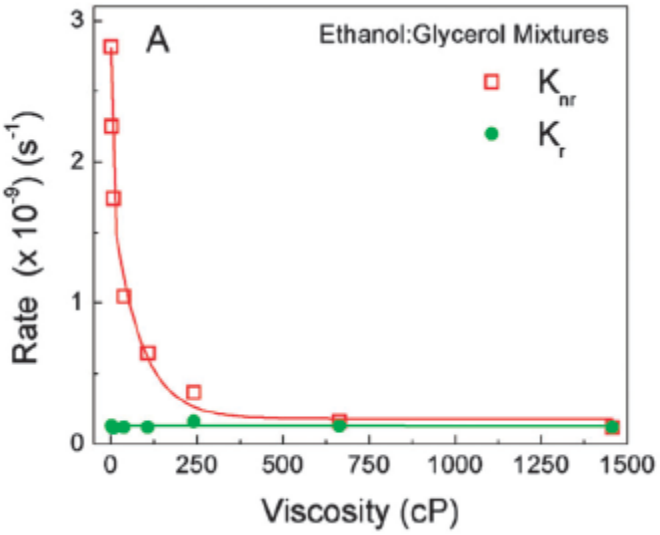

Figure 5.9) Radiative and non-radiative rates of **BD** in ethanol: glycerol mixtures as a function of viscosity.

Moreover, the value of K_r remained steady as a function of the viscosity, however, the value of K_{nr} decreased sharply with increasing viscosity up to 375 cP (Fig. 5.9). This suggested that an increase in quantum yield with increasing viscosity was due to the suppression of non-radiative processes. Although the exact orientation of phenyl rings in relation to the plane of the BODIPY core remains to be clarified, it is arguable that the viscous environment prevented access to the non-emissive state by restricting the rotation of the BODIPY units around the diyne moiety. The complete viscosity dependence was further confirmed by the linear dependence of log quantum yield versus log lifetime (Fig. 5.10).

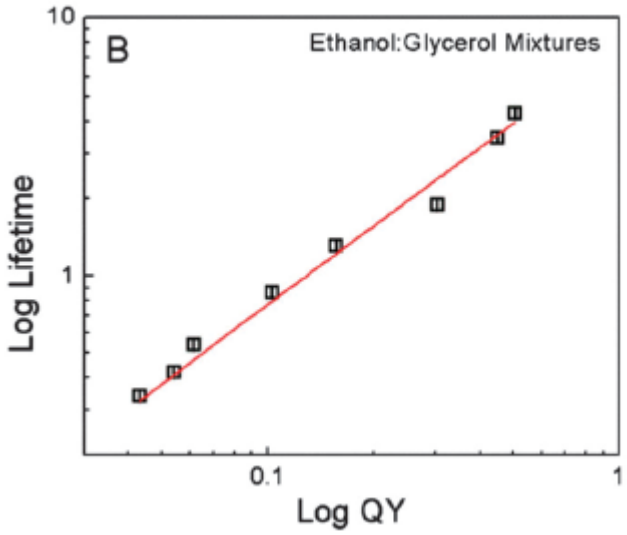

Figure 5.10) log-log plot of the average fluorescence lifetime and quantum yield of **BD** obtained from different ethanol: glycerol mixtures

Evaluating the lifetime of **BD** in the various lipids it appeared that average lifetimes did not vary significantly, except that POPC + cholesterol was found to be longer owing to a comparatively rigid membrane structure (Fig. 5.11). Moreover, examining the lifetime distributions, DPPC indicated the presence of a more ordered lipid structure (as evident from a narrow lifetime distribution) whereby molecules were oriented in a certain (well-ordered) way compared to the other two lipid vesicles. POPC showed a wider lifetime distribution attributed to different micro-viscosities experienced by the BODIPY dimer in vesicles due to less ordered lipid molecules in those vesicles.

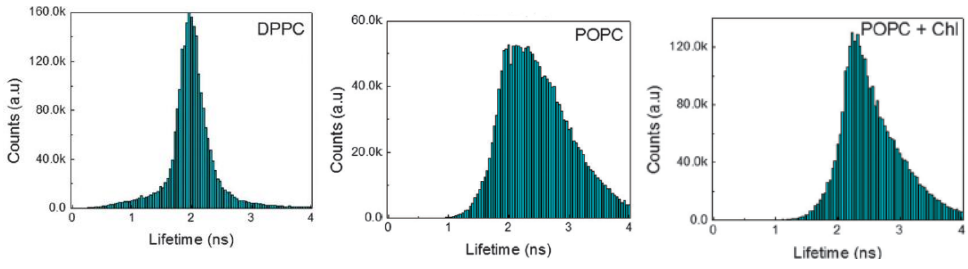

Figure 5.11) Lifetime distrubtion of **BD** from lipid vesicles

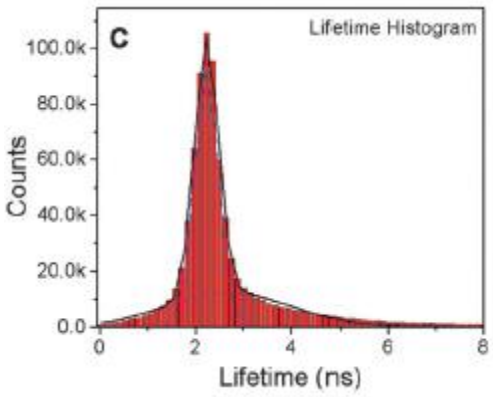

Figure 5.12) Lifetime distribution of SKOV3 cells treated with **BD**

In the SKOV3 cells FLIM image, similar to higher viscosity mixtures (ethanol: glycerol), the fluorescence decay in each pixel could be fitted with a bi-exponential distribution model. We obtained a histogram (Fig. 5.12) of fluorescence lifetimes across the whole image by graphing the lifetime distribution extracted from the Fig. 4.8B. The histogram showed the bi-modal distribution of the dye. By using two Gaussian fits, individual contributions to the histogram were 2.2 ns and 2.6 ns. Such lifetime distributions might indicate two distinctly different dye populations associated with different properties of the environments. A major part (*ca*. 90%) was contributed by 2.2 ns with a narrow FWHM, which was associated with the bright punctate distribution and appears to be located in the vesicular structures. The wider distribution of the lifetime (2.6 ns peak) is due to the random distribution of **BD** inside the cytoplasm and other organelles (distribution of viscosities). The measured fluorescence lifetime inside cells lied within the linear range of the viscosity calibration plot. According to the calibration curve, the 2.2 ns lifetime appeared to the viscosity of *ca*. 260 cP.

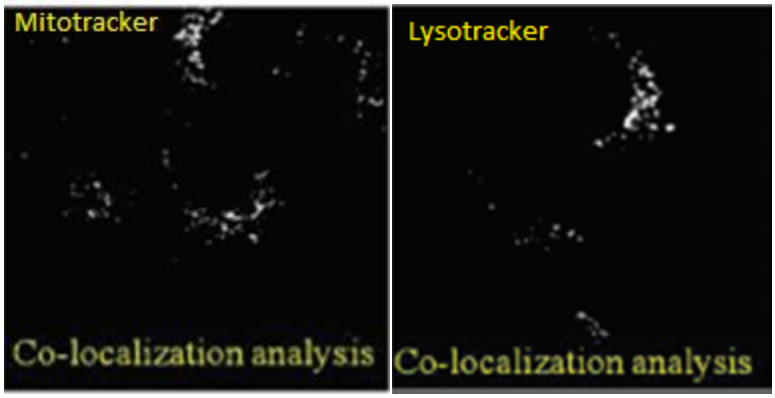

Figure 5.13) Co-localization analysis of **BD** and Mitotracker (left) and Lysotracker (right).

The two individual channels for the **BD** and Mitotracker along with co-localization analysis showed a partial overlap among them (Fig. 5.13 left). Similar results were obtained using Lysotracker and the **BD** (Fig. 5.13 right). These observations suggested that the **BD** also accumulated in organelles other than mitochondria and lysosomes and thus exhibited non-specific cell targeting.

In conclusion, we have reported on a novel, easily accessible homodimeric BODIPY as a steady-state and time-resolved viscosity sensitive molecular rotor-which allowed mapping of the viscosity by non-specifically staining the intracellular organelle. Arguably, structural modifications of the rotor (for example, by incorporating long-alkyl chains onto the BODIPY scaffold) might allow for specific targeting of the cell organelle as well. Considering that the local microviscosity of the plasma membrane/cell organelle is altered in response to external stimuli (oxidants, pore forming agents and signaling events), these molecular viscometers could be suitable for diagnostic applications.

5.4 BODIPY Trimer Molecular Rotor

The large difference in steady-state anisotropy in ethanol for both dyes was due to the difference in their respective fluorescence lifetimes. In ethanol, the lifetime of **T1** (rotor) was short (*ca*. 180 ps), which provided less time for the molecules in the excited state to depolarize the emission via Brownian rotation, thus leading to a relatively higher anisotropy. While in the case of **T2** (non-rotor), the lifetime in ethanol was long (*ca*. 3.4 ns); within this time frame, the fluorescence emission was completely isotropic, which resulted in a low (close to zero) anisotropy. Steady state anisotropy can be used in cellular imaging of viscosity by splitting the emission signal in two different detectors equipped with orthogonal polarizers and thus detecting the respective vertical and perpendicular emission polarization components. This information can be used to calculate the steady state anisotropy across the intensity image.

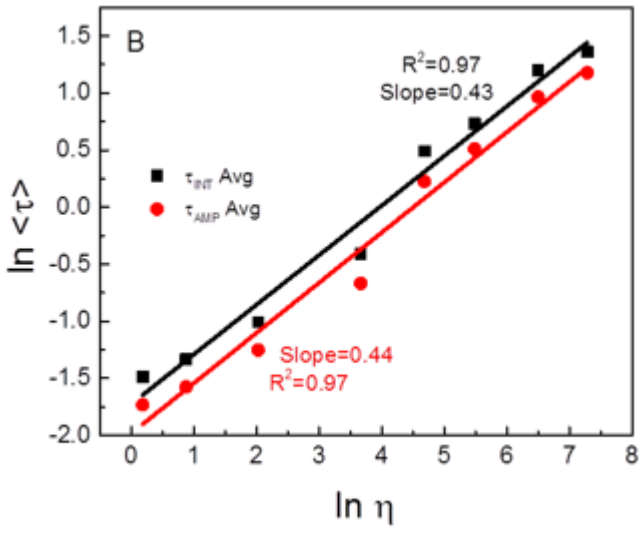

Figure 5.14) log-log plot of **T1**'s average lifetimes vs. viscosity

Based on the fluorescence intensity decays of **T1** in solutions of different viscosities (Fig. 4.13), an obvious change in the slope of decays with an increase in viscosities was noted. *Evaluating the fluorescence lifetime as a function of viscosity (Figure 5.14), suggested that the lifetime of the rotor **T1** changed ca. 18-fold (from 180 ps to 3,245 ps) as the viscosity of media changed from 1.2 cP to 1457 cP. The slope of the linear fit to the rotor data in Fig. 5.14 is 0.43*. This is in good comparison to that of the BODIPY dyad of 0.46. Moreover, it is important to note that the radiative rate, K_r, barely changed (Fig.5.15), while non-radiative rate, K_{nr}, changed by *ca.* 21 times as media's viscosity changed from 1.2 cP to 1457 cP. The fluorescence lifetime only changed by 1.5 times (from 3.44 ns to 4.97 ns) over the same range of viscosities.

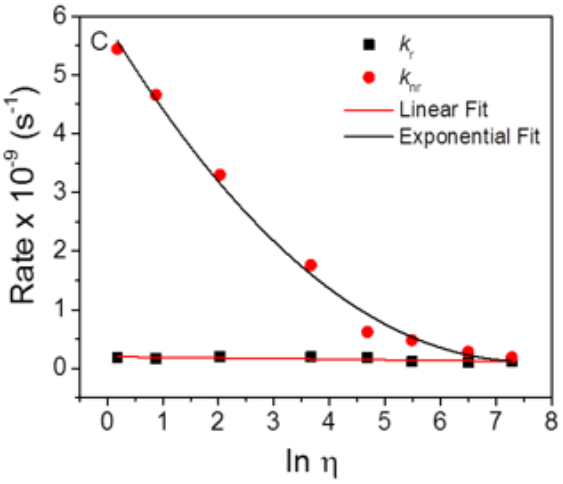

Figure 5.15) Calculated radiative and non-radiative rates of **T1** as a function of viscosity.

Solvents	τ1	τ2	τ3	α1	α2	α3	τ_{Avg} int	τ_{Avg} AMP	χ^2
1-4 Dioxane	0.22	0.52	2.10	0.88	0.11	0.004	0.35	0.27	0.82
2 propanol	0.19	0.58	1.82	0.93	0.06	0.01	0.38	0.24	0.80
Chloroform	0.24	0.51	2.23	0.88	0.11	0.01	0.35	0.27	0.80
Ethanol	0.16	0.62	1.92	0.95	0.04	0.01	0.31	0.19	0.80
Toluene	0.26	0.58	2.16	0.89	0.10	0.01	0.38	0.30	0.80
DCM	0.18	0.45	2.3	0.90	0.097	0.003	0.30	0.21	0.78
Acetone	0.12	0.48	2.4	0.965	0.03	0.005	0.23	0.14	0.80
DMSO	0.18	0.50	1.7	0.876	0.11	0.004	0.34	0.23	0.81

Table 5.1) **T1** lifetime parameters in various polarity solvents

Solvents	τ1	τ2	τ3	α1	α2	α3	τ_{Avg} int	τ_{Avg} AMP	χ^2
1-4 Dioxane	0.24	3.3	4.0	0.04	0.28	0.68	3.8	3.7	0.96
2 propanol	0.25	2.0	3.7	0.05	0.11	0.84	3.6	3.4	0.95
Chloroform	0.19	2.4	3.8	0.03	0.12	0.85	3.7	3.5	0.98
Ethanol	0.26	2.1	3.9	0.06	0.10	0.84	3.8	3.5	1.0
Toluene	0.20	3.1	3.7	0.03	0.44	0.53	3.5	3.3	0.99
DCM	0.29	2.4	3.8	0.05	0.17	0.78	3.6	3.4	0.97
Acetone	0.20	2.5	3.5	0.06	0.35	0.59	3.2	2.95	1.0
DMSO	0.30	2.5	3.7	0.07	0.25	0.68	3.4	3.2	0.97

Table 5.2) **T2** lifetime parameters in various polarity solvents

Further, it is important to consider if polarity of the environment will affect the behavior of the molecular rotor. We tested this by using organic solvents of different polarity and saw minimal change in absorption, fluorescence emission spectra and most importantly- lifetime.(Fig. 4.15 and Tables 5.1 and 5.2). In fact, the lifetime of neither the rotor nor non-rotor displayed any relationship to the dielectric constant. As expected, the rotor's lifetime showed linear agreement ($r^2 = 0.95$) in these solvents. The non-rotor's lifetime also showed marginal linear relation ($r^2 = 0.73$), indicating minimal dependence on viscosity unsurprisingly. This makes us confident that the rotor lifetime

measurement for viscosity determinations will be free from any possible contributions from polarity changes.

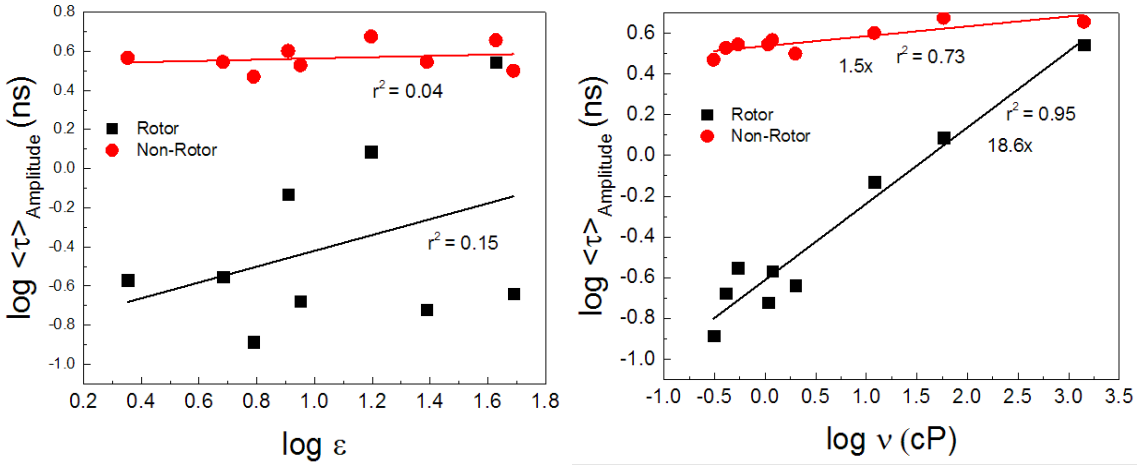

Figure 5.16) Log of **T1** and **T2** lifetime vs. log dielectric constant (left) and log viscosity (right).

5.5 BODIPY Trimer Applications

In the lipids, it is expected that at 15 ° C a gel state would be the dominant form, where the lipid molecules are rigidly packed.[108] Thus, the lateral diffusion of lipid molecules as well as the bond rotations should be suppressed. On the contrary, at 30 ° C a less viscous liquid state would be achieved, where the hydrocarbon chains are expected to be loosely arranged and the bond rotations should be allowed. Based on our data a 1.2 fold change in fluorescence lifetime in case of **T2** could be ascribed to the temperature effect, since the non-rotor molecule is insensitive to viscosity changes that could be induced by temperature. However, the change in case of the rotor molecule **T1** was almost twice owing to changes in the surrounding viscosity along with temperature effect. The measured viscosities of the DMPC vesicles using **T1** were 270,

98 and 60 cP at 15, 23 and 30 ° C, respectively. Arguably, the viscosity measurements (Fig. 4.14) might slightly underestimate the viscosity in lipid bilayer as temperature, which could be viewed as an additional non-radiative channel, would lower the lifetime values as compared to those expected from the viscosity effect alone. Nonetheless, it is plausible that **T1** could be used as molecular viscometer to estimate the viscosity in membrane mimicking vesicles and plasma membranes of various cells.

In the FLIM images (Fig. 4.16), it appeared that the distribution was bimodal in both cancer cell lines: diffuse fluorescence in cytoplasm and bright punctate distribution. *Based on FLIM images the fluorescence lifetime appeared to be long in both areas.*

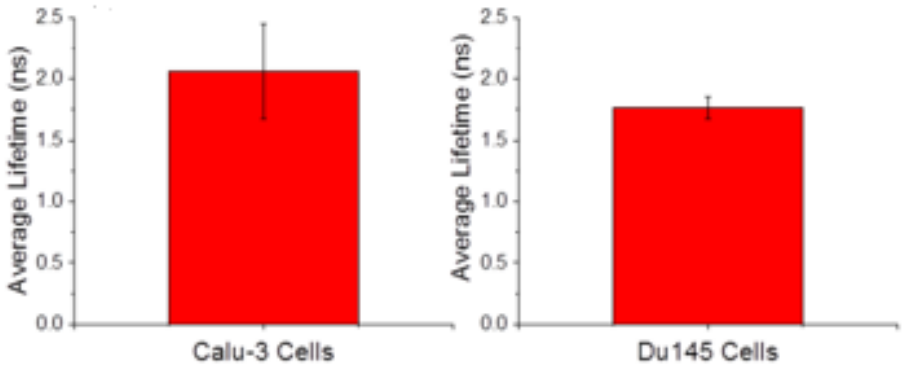

Figure 5.17) Amplitude average lifetime recovered from FLIM images from respective cell lines (n=6 images)

Arguably, this to be attributed to the probe accumulation in membranes of vesicle-like structures (mitochondria, lysosomes, endoplasmic reticulum and Golgi apparatus etc.). A long lifetime and bright fluorescence in these punctate areas are expected due to hydrophobic nature of the dyes as well as due to the high viscosity

surrounding the dye compared to the cytoplasm/aqueous compartment. However, the long lifetime (which is comparable to that observed in the punctate area) in cytoplasm or throughout cells is unusual. As such, an analysis of the lifetime through both the cytoplasm and punctate area was performed for both the Calu 3 (Fig. 5.16) and DU 145 (Fig. 5.17) cell lines.

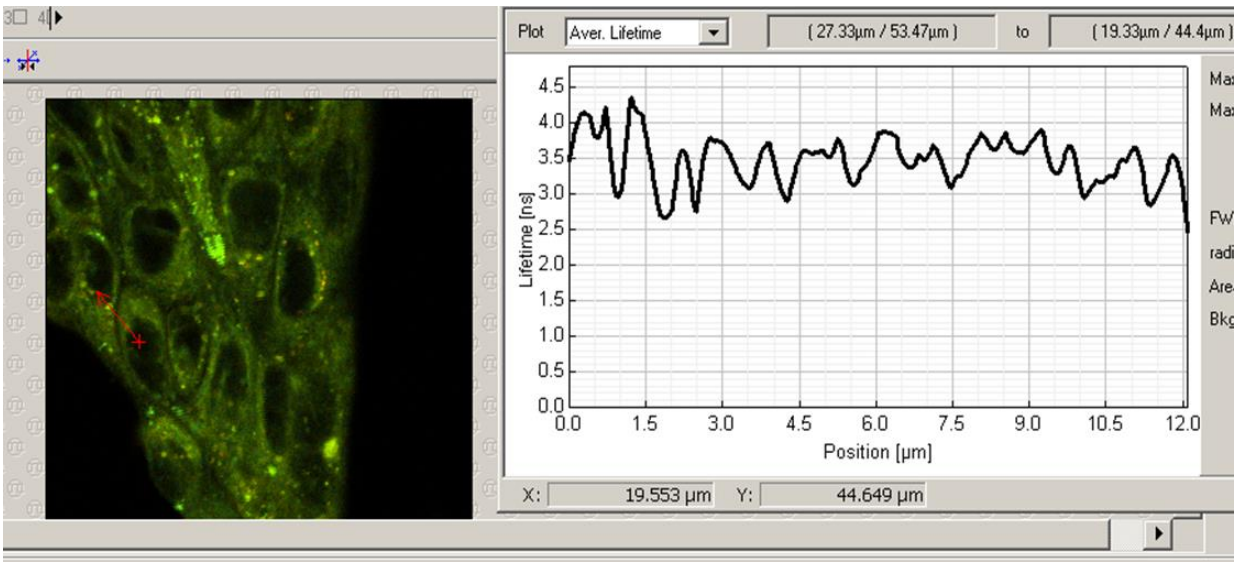

Figure 5.18: FLIM image of Calu 3 cells along with lifetime profile along the red line drawn in the FLIM image. Red line was drawn such that it will pass through cytoplasm and punctate area as well. Lifetime shown on the right is intensity weighted lifetime.

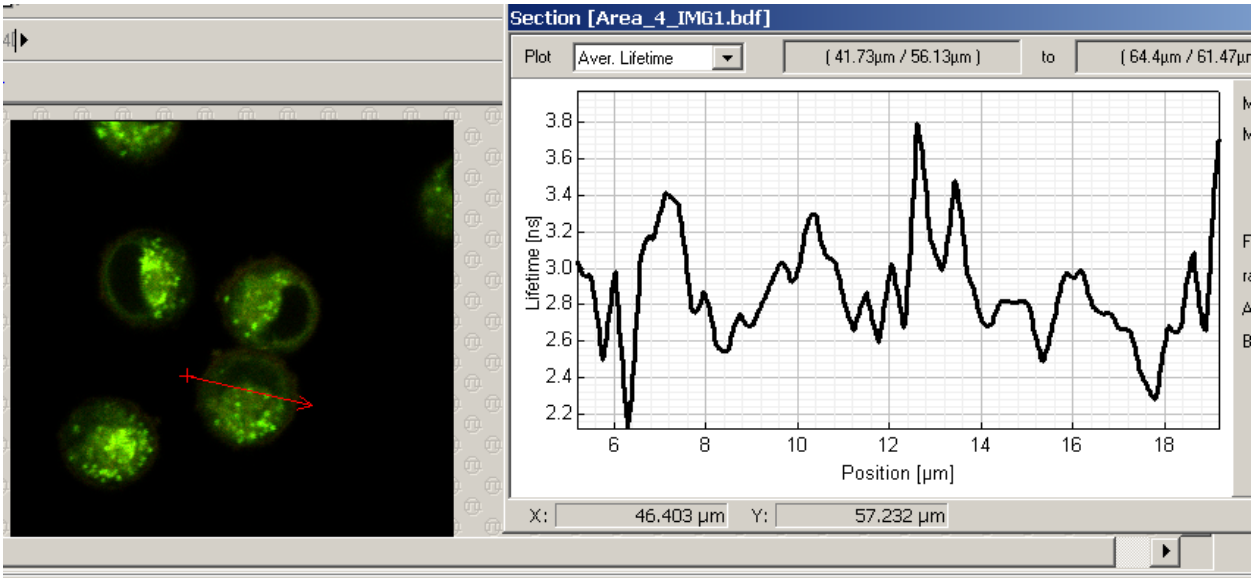

Figure 5.19: FLIM image of DU 145 cells along with lifetime profile along the red line drawn in the FLIM image. Red line was drawn such that it will pass through cytoplasm and punctate area as well. Lifetime shown on the right is intensity weighted lifetime.

Potentially, it could be explained by the binding/physical adsorption of **T1** to the cytoplasmic proteins or other cell components distributed throughout cytoplasm, which would increase the intensity and fluorescence lifetime of the probe by hindering the rotation around the central bond. Cellular cytoplasm has high a concentration of cellular proteins and it provides hydrophobic pockets for dye binding. This hypothesis was tested by studying the binding of rotor to several proteins *in vitro.* Based on the changes of fluorescence lifetime, we found that rotor molecule was adsorbed onto bigger proteins such as bovine serum albumin and human serum albumin but not onto lysozyme. *This information could be crucial in designing viscosity experiments in cellular or biological media.*

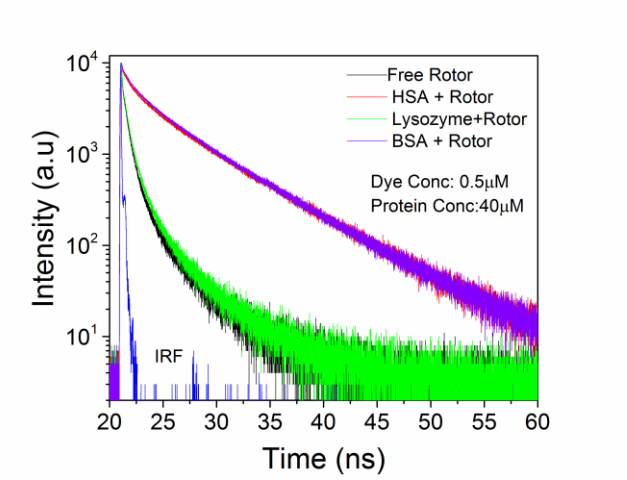

Figure 5.20) Fluorescence intensity decays of **T1** in presence of different proteins.

In summary, we have shown that the triazine-based BODIPY trimer is a high extinction molecular rotor, **T1**, which is able to sense viscosity changes in various environments, including molecular solvents, lipid vesicles and several cancer cell lines. However, analysis of the data in cellular environments should be done with care, since the changes in the fluorescence lifetimes (and subsequently the viscosity estimations) could be affected by binding to various proteins. This problem can be solved by designing targeted fluorophore which will specifically bind to a certain cell organelle or a compartment.

In addition, the fluorescence properties of trimer **T2**, while designed on purpose to not be a molecular rotor, indicated that this dye is potentially a good fluorophore in green region with a high extinction (200,000 $M^{-1} cm^{-1}$) and high quantum yield (0.60)

with comparable lifetime to rhodamine dyes (~ 4 ns). This suggests that triazine could be a valuable scaffold for assembling multichromophoric systems.

Bibliography

1 B. M. Uzhinov, V. L. Ivanov and M. Y. and Melnikov, "Molecular Rotors as luminescence sensors of local viscosity and viscous flow in solutions and organized systems," Russ. Chem. Rev. 80 (12), 1179-1190 (2011).

2 V. T. Turitto, "Blood viscosity, mass transport, and thrombogenesis," Prog.Hemost.Thromb. 6, 139-177 (1982).

3 Y. N. Andrade *et al.*, "TRPV4 channel is involved in the coupling of fluid viscosity changes to epithelial ciliary activity," J.Cell Biol. 168 (6), 869-874 (2005).

4 M. K. Kuimova, "Mapping viscosity in cells using molecular rotors," Phys.Chem.Chem.Phys. 14 (37), 12671-12686 (2012).

5 M. A. Haidekker and E. A. Theodorakis, "Molecular rotors--fluorescent biosensors for viscosity and flow," Org.Biomol.Chem. 5 (11), 1669-1678 (2007).

6 M. A. Haidekker and E. A. Theodorakis, "Environment-sensitive behavior of fluorescent molecular rotors," J.Biol.Eng. 4, 11-1611-4-11 (2010).

7 J. Fan *et al.*, "Energy transfer cassettes based on organic fluorophores: construction and applications in ratiometric sensing," Chem.Soc.Rev. 42 (1), 29-43 (2013).

8 M. Kumar *et al.*, "Naphthalimide appended rhodamine derivative: through bond energy transfer for sensing of Hg2+ ions," Org.Lett. 13 (6), 1422-1425 (2011).

9 X. Cao *et al.*, "Ratiometric sensing of fluoride anions based on a BODIPY-coumarin platform," Org.Lett. 13 (22), 6098-6101 (2011).

10 Haibo Yu *et al.*, "Convenient and Efficient FRET Platform Featuring a Rigid Biphenyl Spacer between Rhodamine and BODIPY: Transformation of 'Turn-On' Sensors into Ratiometric Ones with Dual Emission," Chemistry – A European Journal 17 (11), 3179-3191 (2011).

11 J. P. Hallett and T. Welton, "Room-temperature ionic liquids: solvents for synthesis and catalysis. 2," Chem.Rev. 111 (5), 3508-3576 (2011).

12 M. H. G. Pretchtl and S. and Sahler, "Hydrogen storage using ionic liquid media," Cur. Org. Chem. 17, 220-228 (2013).

13 Z. Fei and P. J. Dyson, "The making of iLiquids--the chemist's equivalent of the iPhone," Chem.Commun.(Camb) 49 (26), 2594-2596 (2013).

14 A. Brandt *et al.*, "Deconstruction of lignocellulosic biomass with ionic liquids," Green Chem. 15, 550-583 (2013).

15 X. Sun, H. Luo and S. Dai, "Ionic liquids-based extraction: a promising strategy for the advanced nuclear fuel cycle," Chem.Rev. 112 (4), 2100-2128 (2012).

16 T. L. Greraves and C. J. Drummond, "Solvent nanostructure, the solvophobic effect and amphiphile self-assembly in ionic liquids," Chem.Soc.Rev. 42 (3), 1096-1120 (2013).

17 H. Weingartner, C. Cabrele and C. Herrmann, "How ionic liquids can help to stabilize native proteins," Phys.Chem.Chem.Phys. 14 (2), 415-426 (2012).

18 C. Chiappe and D. and Pieraccini, "Ionic liquids: solvent properties and organic reactivity," J. Phys.Org. Chem. 18, 275-297 (2005).

19 I. Newington, J. M. Perez-Arlandis and T. Welton, "Ionic liquids as designer solvents for nucleophilic aromatic substitutions," Org.Lett. 9 (25), 5247-5250 (2007).

20 M. J. Earle, S. P. Katdare and K. R. Seddon, "Paradigm confirmed: the first use of ionic liquids to dramatically influence the outcome of chemical reactions," Org.Lett. 6 (5), 707-710 (2004).

21 S. V. Dzyuba and R. A. and Bartsch, "Expanding the polarity range of ionic liquids," Tetrahedron Lett. 43 (26), 4657-4659 (2002).

22 L. P. Jameson and S. V. Dzyuba, "Spectroscopic studies on tetracycline in room-temperature ionic liquids," J.Nat.Prod. 74 (3), 310-313 (2011).

23 L. P. Jameson and S. and Dzyuba, "Ionic liquid-controlled conformational bias of tetracycline," RSC Adv. 3, 4582-4587 (2013).

24 V. Kumar, G. A. Baker and S. Pandey, "Ionic liquid-controlled J- versus H-aggregation of cyanine dyes," Chem.Commun. 47 (16), 4730-4732 (2011).

25 D. C. Khara *et al.*, "Effect of the alkyl chain length on the rotational dynamics of nonpolar and dipolar solutes in a series of N-alkyl-N-methylmorpholinium ionic liquids," J. Phys. Chem. B. 117 (17), 5156-5164 (2013).

26 S. Mandal *et al.*, "Roles of viscosity, polarity, and hydrogen-bonding ability of a pyrrolidinium ionic liquid and its binary mixtures in the photophysics and rotational dynamics of the potent excited-state intramolecular proton-transfer probe 2,2'-bipyridine-3,3'-diol," J. Phys. Chem. B. 117 (22), 6789-6800 (2013).

27 B. Li *et al.*, "Spectroscopic evidence for unusual microviscosity in imidazolium ionic liquid and tetraethylene glycol dimethyl ether cosolvent mixtures," J. Phys. Chem. B. 116 (44), 13272-13281 (2012).

28 S. Pandey *et al.*, "Fluorescent probe studies of polarity and solvation within room temperature ionic liquids: a review," J.Fluoresc. 22 (5), 1313-1343 (2012).

29 M. Balaz *et al.*, "Synthesis of hydrophilic conjugated porphyrin dimers for one-photon and two-photon photodynamic therapy at NIR wavelengths," Org. Biomole. Chem. 7 (5), 874-888 (2009).

30 M. K. Kuimova *et al.*, "Imaging intracellular viscosity of a single cell during photoinduced cell death," Nat.Chem. 1 (1), 69-73 (2009).

31 M. A. Haidekker *et al.*, "A ratiometric fluorescent viscosity sensor," J.Am.Chem.Soc. 128 (2), 398-399 (2006).

32 Alfred Treibs and Franz-Heinrich Kreuzer, "Difluorboryl-Komplexe von Di- und Tripyrrylmethenen," Justus Liebigs Ann.Chem. 718 (1), 208-223 (1968).

33 A. Loudet and K. Burgess, "BODIPY dyes and their derivatives: syntheses and spectroscopic properties," Chem.Rev. 107 (11), 4891-4932 (2007).

34 G. Ulrich, R. Ziessel and A. Harriman, "The chemistry of fluorescent bodipy dyes: versatility unsurpassed," Angew.Chem.Int.Ed Engl. 47 (7), 1184-1201 (2008).

35 H. Lu *et al.*, "Structural modification strategies for the rational design of red/NIR region BODIPYs," Chem.Soc.Rev. 43 (13), 4778-4823 (2014).

36 M. K. Kuimova, "Mapping viscosity in cells using molecular rotors," Phys. Chem. Chem. Phys. 14, 12671-12686 (2012).

37 H. L. Kee *et al.*, "Structural control of the photodynamics of boron-dipyrrin complexes," J Phys Chem B 109 (43), 20433-20443 (2005).

38 M. K. Kuimova *et al.*, "Molecular rotor measures viscosity of live cells via fluorescence lifetime imaging," J.Am.Chem.Soc. 130 (21), 6672-6673 (2008).

39 Y. Wu *et al.*, "Molecular rheometry: direct determination of viscosity in Lo and Ld lipid phases via fluorescence lifetime imaging," Phys.Chem.Chem.Phys. 15 (36), 14986-14993 (2013).

40 I. Lopez-Duarte *et al.*, "A molecular rotor for measuring viscosity in plasma membranes of live cells," Chem.Commun. 50 (40), 5282-5284 (2014).

41 H. Zhu *et al.*, "A "distorted-BODIPY"-based fluorescent probe for imaging of cellular viscosity in live cells," Eur. J. Chem. 20 (16), 4691-4696 (2014).

42 L. Wang *et al.*, "Activatable rotor for quantifying lysosomal viscosity in living cells," J.Am.Chem.Soc. 135 (8), 2903-2906 (2013).

43 H. L. Kee *et al.*, "Structural control of the photodynamics of boron-dipyrrin complexes," J. Phys. Chem. B. 109 (43), 20433-20443 (2005).

44 Y. Wu *et al.*, "Molecular rheometry: direct determination of viscosity in Lo and Ld lipid phases via fluorescence lifetime imaging," Phys.Chem.Chem.Phys. 15 (36), 14986-14993 (2013).

45 I. Lopez-Duarte *et al.*, "A molecular rotor for measuring viscosity in plasma membranes of live cells," Chem.Commun.. 50 (40), 5282-5284 (2014).

46 H. Zhu *et al.*, "A "distorted-BODIPY"-based fluorescent probe for imaging of cellular viscosity in live cells," Eur. J. Chem. 20 (16), 4691-4696 (2014).

47 M. A. H. Alamiry *et al.*, "Fluorescent molecular rotors under pressure: synergistic effects of an inert polymer," RSC Adv. 2, 9851-9859 (2012).

48 D. Wang *et al.*, "BODIPY-conjugated thermoresponsive copolymer as a fluorescent thermometer based on polymer microviscosity," Langmuir 25 (22), 13176-13182 (2009).

49 E. Bahaidarah *et al.*, "Fluorescent molecular rotors based on the BODIPY motif: effect of remote substituents," Photochem.Photobiol.Sci. 13 (10), 1397-1401 (2014).

50 X. Yin *et al.*, "A highly sensitive viscosity probe based on ferrocene-BODIPY dyads," Dalton Trans. 39 (41), 9929-9935 (2010).

51 Z. Yang *et al.*, "A self-calibrating bipartite viscosity sensor for mitochondria," J.Am.Chem.Soc. 135 (24), 9181-9185 (2013).

52 Z. Yang *et al.*, "A Nile Red/BODIPY-based bimodal probe sensitive to changes in the micropolarity and microviscosity of the endoplasmic reticulum," Chem.Commun. 50 (79), 11672-11675 (2014).

53 G. Ulrich, R. Ziessel and A. Harriman, "The chemistry of fluorescent bodipy dyes: versatility unsurpassed," Angew.Chem.Int.Ed Engl. 47 (7), 1184-1201 (2008).

54 Raymond Ziessel, Gilles Ulrich and Anthony and Harriman, "The chemistry of Bodipy: A new El Dorado for fluorescence tools," New J. Chem. 31 (4), 496-501 (2007).

55 N. Boens, V. Leen and W. Dehaen, "Fluorescent indicators based on BODIPY," Chem.Soc.Rev. 41 (3), 1130-1172 (2012).

56 Aurore Loudet and Kevin Burgess, "BODIPY dyes and their derivatives: syntheses and spectroscopic properties," Chem.Rev. 107 (11), 4891-4932 (2007).

57 A. Kamkaew *et al.*, "BODIPY dyes in photodynamic therapy," Chem. Soc. Rev. 42 (1), 77 (2013).

58 A. C. Benniston and G. Copley, "Lighting the way ahead with boron dipyrromethene (Bodipy) dyes," Phys.Chem.Chem.Phys. 11 (21), 4124-4131 (2009).

59 J. A. Levitt *et al.*, "Fluorescence anisotropy of molecular rotors," Chem.Phys.Chem. 12 (3), 662-672 (2011).

60 J. A. Levitt *et al.*, "Membrane-Bound Molecular Rotors Measure Viscosity in Live Cells via Fluorescence Lifetime Imaging." J. Phys. Chemi. C 113 (27), 11634-11642 (2009).

61 J. Kimball *et al.*, "BODIPY-BODIPY dyad: assessing the potential as a viscometer for molecular and ionic liquids," Royal Society of Chemsitry Advances 5 (25), 19508 (2015).

62 S. Raut *et al.*, "A homodimeric BODIPY rotor as a fluorescent viscosity sensor for membrane-mimicking and cellular environments," Phys.Chem.Chem.Phys. 16 (48), 27037-27042 (2014).

63 D. C. Harris and M. D. and Bertolucci, Symmetry and Spectroscopy: An introduction to vibrational and electronic spectroscopy, edited by Anonymous (Dover Publications, Inc., New York, 1978), .

64 A. Einstein, "Plancksche theorie der strahlung und die theorie der spezifischen warme," Annalen der Physik 22, 180-190 (1907).

65 L. Eyges, The classical electromagnetic field, edited by Anonymous 1st ed. (Dover Publications, Inc., New York, 1972), .

66 M. Born and J. R. and Oppenheimer, "Zur quantentheorie der molekeln," Annalen der Physik 84, 457-484 (1927).

67 J. Lakowicz, Principles of Fluorescence Spectroscopy, edited by Anonymous 3rd ed. (Springer, New York, NY, USA, 2006), .

68 Z. R. Grabowski, K. Rotkiewicz and W. and Retting, "Structual changes accompanying intramolecular electron transfer: focus on twisted intramolecular charge-transfer states and structures," Chem. Rev.103, 3899-4031 (2003).

69 A. K. Dutta, K. Kamada and K. and Ohta, "Spectroscopic studies of Nile red in organic solvents and polymers," J. Photochemistry & Photobiology, A: Chemistry 93, 57-64 (1996).

70 K. Y. Law, "Fluorescence probe for microenvironments: anomalous viscosity dependence of the fluorescence quantum yield of p-N,N-

Dialkylaminobenzylidenemalononitrile in 1-Alkanols," Chem.Phys. Lett. 75 (3), 545-549 (1980).

71 T. Forster and G. and Hoffmann, "Effect of viscosity on the fluorescence quantum yield of some dye systems," Zeitschrift für Physikalische Chemie 75, 63-76 (1971).

72 A. F. Lopez, O. P. Ruiz and A. I. and Lopez, "On the aggregation of rhodamine b in ethanol," Chem. Phys. Lett. 148 (2), 253-258 (1988).

73 I. Gryczynski *et al.*, Nonlinear Curve-Fitting Methods for Time-Resolved Data Analysis, in FLIM Microscopy in Biology and Medicine, edited by A. Periasamy and R. and Clegg, (Chapman and Hall/CRC, 2009), pp. 472.

74 A. Ahosseini and A. M. and Scurto, "Viscosity of imidazolium-based ionic liquids at elevated pressures: cation and anion effects," Int. J. Thermophys. 29 (4), 1222-1243 (2008).

75 H. Shirota *et al.*, "Comparison between dicationic and monocationic ionic liquids: liquid density, thermal properties, surface tension and shear viscosity," J. Chem. Eng. Data 56 (5), 2453-2459 (2011).

76 S. V. Dzyuba and R. A. and Bartsch, "Influence of structural variations in 1-alkyl(aralkyl)-3-methylimidazolium hexafluorophosphates and

bis(trifluoromethylsulfonyl)imides on physical properties of the ionic liquids," Chem.Phys.Chem. 3 (2), 161-166 (2002).

77 B. Mokhtarani *et al.*, "Density and viscosity of 1-butyl-3-methylimidazolium nitrate with ethanol, 1-propanol, or 1-butanol at several temperatures," J. Chem. Thermodyn.41 (12), 1432-1438 (2009).

78 J. G. Huddleston *et al.*, "Characterization and comparison of hydrophilic and hydrophobic room temperature ionic liquids incorporating the imidazolium cation," Green Chem. 3, 156-164 (2001).

79 K. R. Seddon, A. Stark and M. J. and Torres, "Influence of chloride, water, and organic solvents on the physical properties of ionic liquids," Pure App. Chem. 72 (12), 2275-2287 (2009).

80 P. K. Mandal and A. Samanta, "Fluorescence studies in a pyrrolidinium ionic liquid: polarity of the medium and solvation dynamics," J. Phys. Chem. B. 109 (31), 15172-15177 (2005).

81 A. Samanta, "Solvation dynamics in ionic liquids: what we have learned from the dynamic fluorescence Stokes Shift studies," J.Phys. Chem. Lett. 1 (10), 1557-1562 (2010).

82 N. W. Smith *et al.*, "Triazole-containing BODIPY dyes as novel fluorescent probes for soluble oligomers of amyloid Abeta1-42 peptide," Biochem.Biophys.Res.Commun. 391 (3), 1455-1458 (2010).

83 L. Jameson and S. and Dzyuba, "Expedious, mechanochemical synthesis of BODIPY dyes," Beilstein J. Org. Chem. 9, 786 (2013).

84 P. Siemsen, R. C. Livingston and F. Diederich, "Acetylenic Coupling: A Powerful Tool in Molecular Construction," Angew.Chem.Int.Ed Engl. 39 (15), 2632-2657 (2000).

85 N. W. Smith *et al.*, "Base and concentration effects on the product distribution in copper-promoted alkyne-azide cycloaddition: additive-free route to 5-iodo-triazoles." Tetrahedron Lett. 51, 550-553 (2010).

86 M. Smiglak, A. Metlen and R. D. Rogers, "The second evolution of ionic liquids: from solvents and separations to advanced materials--energetic examples from the ionic liquid cookbook," Acc.Chem.Res. 40 (11), 1182-1192 (2007).

87 M. Petkovic *et al.*, "Ionic liquids: a pathway to environmental acceptability," Chem.Soc.Rev. 40 (3), 1383-1403 (2011).

88 Q. Zhang and J. M. Shreeve, "Ionic liquid propellants: future fuels for space propulsion," Eur. J. Chem. 19 (46), 15446-15451 (2013).

89 J. S. Wilkes, "Properties of ionic liquid solvents for catalysis," J. Mol. Catal A: Chem.214 (1), 11-17 (2004).

90 S. V. Dzyuba and R. A. Bartsch, "Influence of structural variations in 1-alkyl(aralkyl)-3-methylimidazolium hexafluorophosphates and bis(trifluoromethyl-sulfonyl)imides on physical properties of the ionic liquids," Chem. Phys Chem. 3 (2), 161-166 (2002).

91 G. Yu *et al.*, "Viscosity of ionic liquids:database, observation, and quantatative structure-property relationship analysis," AIChe Journal 58, 2885-2899 (2012).

92 S. Chen *et al.*, "Ionic liquid clusters: structure, formation mechanism, and effect on the behavior of ionic liquids," Phys.Chem.Chem.Phys. 16 (13), 5893-5906 (2014).

93 J. Dupont, "From molten salts to ionic liquids: a "nano" journey," Acc.Chem.Res. 44 (11), 1223-1231 (2011).

94 M. C. Corvo *et al.*, "Solvation of carbon dioxide in [C4 mim][BF(4)] and [C(4) mim][PF(6)] ionic liquids revealed by high-pressure NMR spectroscopy," Angew.Chem.Int.Ed Engl. 52 (49), 13024-13027 (2013).

95 Y. Wang and G. A. Voth, "Unique spatial heterogeneity in ionic liquids," J.Am.Chem.Soc. 127 (35), 12192-12193 (2005).

96 O. Russina *et al.*, "Mesoscopic structural organization in triphilic room temperature ionic liquids," Faraday Discuss. 167, 499-513 (2013).

97 N. Tripathi and S. and Saha, "Unravelling the heterogeneity in n butyl-n-methylpiperidinium trifluro methanesulfonimide ionic liquid by 1D and 2D NMR Spectroscopy," Chem. Phys. Lett. 607, 57-63 (2014).

98 C. C. Weber, A. F. Masters and T. Maschmeyer, "Steric, hydrogen-bonding and structural heterogeneity effects on the nucleophilic substitution of N-(p-fluorophenyldiphenylmethyl)-4-picolinium chloride in ionic liquids," Org.Biomol.Chem. 11 (15), 2534-2542 (2013).

99 C. C. Weber, A. F. Masters and T. Maschmeyer, "Pseudo-encapsulation--nanodomains for enhanced reactivity in ionic liquids," Angew.Chem.Int.Ed Engl. 51 (46), 11483-11486 (2012).

100 L. P. Jameson *et al.*, "Effect of ionic liquids on the conformation of a porphyrin-based viscometer," RSC Adv.s 3, 18300-18304 (2013).

101 K. Suhling, P. M. French and D. Phillips, "Time-resolved fluorescence microscopy," Photochem.Photobiol.Sci. 4 (1), 13-22 (2005).

102 M. K. Kuimova *et al.*, "Imaging intracellular viscosity of a single cell during photoinduced cell death," Nat.Chem. 1 (1), 69-73 (2009).

103 A. Paul and A. Samanta, "Free volume dependence of the internal rotation of a molecular rotor probe in room temperature ionic liquids," J Phys Chem B 112 (51), 16626-16632 (2008).

104 O. Russina *et al.*, "Mesoscopic structural heterogeneities in room-temperature ionic liquids," J.Phys. Chem. Lett. 3 (1), 27-33 (2012).

105 S. Raut *et al.*, "A homodimeric BODIPY rotor as a fluorescent viscosity sensor for membrane-mimicking and cellular environments," Phys. Chem. Chem. Phys. 16 (48), 27037 (2014).

106 M. Kaschke, J. Kleinschmidt and B. and Wilhelmi, "Computer simulations of viscosity dependent molecular relaxation processes," Laser Chem. 5, 119-132 (1985).

107 J. R. Silvius, Lipid-Protein Interactions, (Jon Wiley & Sons, Inc., New York, 1982),

Note: Passages in this thesis have been quoted verbatim from the following sources:

J. Kimball *et al.*, "BODIPY-BODIPY dyad: assessing the potential as a viscometer for molecular and ionic liquids," RSC Adv. 5 (25), 19508 (2015).

L. P. Jameson *et al.*, "Effect of ionic liquids on the conformation of a porphyrin-based viscometer," RSC Adv. 3, 18300-18304 (2013).

S. Raut *et al.*, "A homodimeric BODIPY rotor as a fluorescent viscosity sensor for membrane-mimicking and cellular environments," Phys. Chem. Chem. Phys. 16 (48), 27037 (2014).

Vita

Personal Background	Joseph Daniel Kimball III
	Monroeville, PA
	Son of Joseph and Colleen Cahill Kimball, Jr.
Education	Diploma, Manistee High School, Manistee, MI, 2006
	Bachelor of Science, Physics, Michigan State University
	East Lansing, MI, USA, 2010
	Doctor of Philosophy, Physics, Texas Christian University
	Fort Worth, TX, USA, 2015
Experience	Research Assistantship, Texas Christian University,
	Fort Worth, TX, USA 2014-2015
	Teaching Assistantship, Texas Christian University
	Fort Worth, TX, USA, 2011-2015
	Student Research Volunteer, UNT Health Science Center
	Fort Worth, TX, USA, 2011-2015
	Undergraduate Research, Michigan State University
	East Lansing, MI, USA, 2008-2010
Awards	Inaugural TCU 3 Minute Thesis Competition
	2015, Judge's 1st Place, People's Choice 1st Place
	Research Stipend
	2015, NIH Grant RO1EB12003
	Student Teacher of the Year,
	2012,2013, TCU College of Science and Engineering
Professional Memberships	Society of Physics Students, Biophysics, SPIE, APS

ABSTRACT

PORPHYRIN AND BODIPY MOLECULAR ROTORS AS MICROVISCOMETERS

By Joseph Daniel Kimball III, Ph.D., 2015

Department of Physics and Astronomy

Texas Christian University

Dissertation Advisor:

Dr. Zygmunt Gryczynski, W.A. "Tex" Moncrief Jr. Chair Professor of Physics

Committee Members:

Dr. Sergei Dzyuba, Associate Professor of Chemistry

Dr. Peter Frinchaboy, Associate Professor of Physics

Dr. Anton Naumov, Assistant Professor of Physics

Viscosity, a fluid's internal resistance to flow and resist molecular diffusion, is a fundamental property of fluid media. Determining the bulk viscosity of a fluid has been easy to relatively simple to accomplish for many years, yet in the recent decade there has been a focus on techniques to measure a fluid's microviscosity. Microviscosity differs from bulk viscosity such that microviscosity is the friction experienced by a single particle interacting with its micron-sized local environment. Macroscopic methods to evaluate the viscosity are well established, but methods to determine viscosity on the microscale level remains unclear.

This work determines the viability of three molecular rotors designed as probes for microviscosity in organic media, ionic liquids, and in the cellular microenvironment. Understanding microviscosity is important because it one of the main properties of any fluid and thus has an effect on any diffusion related processes. A variety of mass and signal transport phenomena as well as intermolecular interactions are often governed by viscosity.

Molecular rotors are a subclass of intramolecular charge transfer fluorophores which form a lower energy twisted state. This results in a charge separated species which is highly sensitive to its surrounding microenviroment's viscosity as high viscosity limits its ability to form this twisted state. Once excited, there are deactivation routes which the excited fluorophore can undergo: radiative and non-radiative. Both were studied in this work.

In the case of a radiative decay, as seen in porphyrin dimer, the energy is released in the form of a photon and is seen as a shifted band in the emission structure. The conformation of the porphyrin dimer was found to be *influenced differently by ionic liquids as compared to molecular solvents*, indicating the microheterogenous nature of ionic liquids play a role in the conformation.

For non-radiative decays, BODIPY dyads and triads were investigated. The triad has an extinction coefficient in the range of *200,000* M^{-1} cm^{-1}, making it an extremely

useful and sensitive fluorescent molecular rotor. Their fluorescent lifetimes were proven to correlate linearly with viscosity. Thus they were both encapsulated into lipds to determine their viability for cellular studies.

The dyes were readily uptaken into three cancer cell lines, SKOV3, Calu 3 and Du 145. The lifetimes were then recorded using FLIM to map the viscosity of the cellular cytoplasm, mitochondria, lysosomes and other various organelles. A longer than expected lifetime in the cytoplasm was observed. This could be due to binding onto cytoplasmic proteins distributed throughout the cytoplasm, *not due to viscosity as the theory of molecular rotors predicts.*